上海交通大学“学术之星”评选

通讯评审材料

申请方向 _____化学_____

推荐单位 ___化学化工学院_____

填表日期 _____0161008_____

上海交通大学“学术之星”评选组委会 制表

目　录

1. 代表性论文、专利、论著情况

<table>
<tr><td colspan="3">本栏目请填写申请人的代表性成果及他人对其成果的评价和引用情况，
（所列论文数不超过 3 篇，专著不超过 3 本，专利不超过 3 项）</td></tr>
<tr><td rowspan="6">论文</td><td colspan="2">论文 1：
Temperature-Dependent Multidimensional Self-Assembly of Polyphenylene-Based “Rod−Coil” Graft Polymers.
J. Am. Chem. Soc. 2015, 137, 11602−11605.</td></tr>
<tr><td>贡献度: √主要完成人 □次要完成人 □参与人</td><td>第一作者</td></tr>
<tr><td colspan="2">论文 2：
Poly(ethylene oxide) Functionalized Graphene Nanoribbons with Excellent Solution Processability.
J. Am. Chem. Soc., 2016, 138, 10136–10139.</td></tr>
<tr><td>贡献度: √主要完成人 □次要完成人 □参与人</td><td>第一作者</td></tr>
<tr><td colspan="2">论文 3：
Ultra-large sheet formation by 1D to 2D hierarchical self-assembly of a “rod–coil” graft copolymer with a polyphenylene backbone.Polym. Chem., 2016, 7, 1234–1238.</td></tr>
<tr><td>贡献度: √主要完成人 □次要完成人 □参与人</td><td>第一作者</td></tr>
<tr><td>他人引用及评价情况(不多于 5 条评价，限 400 字,)</td><td colspan="2">他人对论文1 的评价：
（1）此工作设计合成了以聚苯为骨架的“Rod-coil”型刷状聚合物，设计思路和合成路线很有参考价值；
（2）研究了“Rod-coil”型刷状聚合物自组装行为，非手性的聚合物呈现出非凡的自组装行为，即在特定的条件下能形成螺旋线。刷状聚合物的这种组装行为还从未被报道。
他人对论文2 的评价：
（1）这是一篇很出色的工作，合成了结构精确的具有椅型边缘的石墨烯纳米带（GNR），其宽1-1.7 nm，长15-60 nm，合成路线很值得参考。
（2）此工作很好的展现了聚合物功能化对GNR 在常用溶剂中的分散性的影响，并使GNR 在四氢呋喃中能达到很高的分散浓度（骨架浓度1 mg/mL）。基于它的优异分散性，作者得以展开GNRs 在溶液中的性质研究或需要溶液加工的应用考察，如GNR-thin-film 场效应晶体管。</td></tr>
</table>

<table>
<tr><td rowspan="6">论著</td><td colspan="2">论著 1：</td></tr>
<tr><td>负责完成　章节，共　万字</td><td>第□作者</td></tr>
<tr><td colspan="2">论著 2：</td></tr>
<tr><td>负责完成　章节，共　万字</td><td>第□作者</td></tr>
<tr><td colspan="2">论著 3：</td></tr>
<tr><td>负责完成　章节，共　万字</td><td>第□作者</td></tr>
<tr><td>论著受资助及获奖情况</td><td colspan="2"></td></tr>
<tr><td rowspan="6">专利</td><td colspan="2">专利 1：
一种碗状氮掺杂碳中空粒子的制备方法及应用。
[P] 公布号：CN105551831A，2016。</td></tr>
<tr><td>贡献度:□主要完成人 □次要完成人 √参与人</td><td>第七完成人</td></tr>
<tr><td colspan="2">专利 2：
一种孔径大小可控的介孔碳球材料的制备方法。
[P] 公布号：CN105523540A，2016。</td></tr>
<tr><td>贡献度:□主要完成人 □次要完成人 √参与人</td><td>第六完成人</td></tr>
<tr><td colspan="2">专利 3：</td></tr>
<tr><td>贡献度:□主要完成人 □次要完成人 □参与人</td><td>第□完成人</td></tr>
<tr><td>专利转化情况</td><td colspan="2"></td></tr>
</table>

JACS
JOURNAL OF THE AMERICAN CHEMICAL SOCIETY

Communication

pubs.acs.org/JACS

Temperature-Dependent Multidimensional Self-Assembly of Polyphenylene-Based "Rod−Coil" Graft Polymers

[†]School of Chemistry and Chemical Engineering, Shanghai Jiao Tong University, 800 Dongchuan RD, Shanghai 200240, P. R. China
[‡]Max Planck Institute for Polymer Research, Ackermannweg 10, 55128 Mainz, Germany
[§]Department of Chemistry and Food Chemistry, Technische Universität Dresden, Mommsenstrasse 4, 01062 Dresden, Germany

Supporting Information

ABSTRACT: We present a novel type of "rod−coil" graft copolymer containing a polyphenylene backbone linked with poly(ethylene oxide) (PEO) side chains. Such graft copolymers manifest unprecedented temperature-dependent one-dimensional (1D) and two-dimensional (2D) self-assembly in solution. At 20 °C, which is higher than the crystallization temperature (T_c) of the PEO chains, the achiral graft copolymers self-organize into nanoribbons that twist into ∼30 μm ultralong helices with controlled pitch depending on the grafting ratio of the PEO chains. At 10 °C, which is lower than the T_c, quadrangular multilayer sheets of over 10 μm in lateral size are obtained. To our knowledge, this work presents the first example of controlled self-assembly of graft polymers into 1D helix and 2D sheet superstructures.

The supramolecular nanostructures of conjugated polymers with rigid backbones,[1] e.g., polyphenylene and polythiophene, have attracted considerable interest, owing to their unique electronic and optoelectronic properties.[1−7] In general, "rod−coil" conjugated polymers with both rigid conjugated and flexible polymer sequences can be synthons for self-assembly, the two primary types of which are rod−coil block copolymers and rod−coil graft copolymers. The self-assembly of rod−coil block copolymers has been extensively investigated in the past, and various ordered nanostructures, including spheres, cylinders, and vesicles, have been achieved.[2−7] For instance, Park and coworkers reported the self-assembly of a polythiophene-based rod−coil block copolymer, namely, poly[3-(2,5,8,11-tetraoxatridecanyl)-thiophene]-*block*-poly(ethylene glycol), resulting in ribbons and vesicles in tetrahydrofuran (THF)−water solutions depending on the water content.[7] In contrast, although the self-assembly of rod−coil graft copolymers, which comprise a rigid conjugated backbone with densely tethered polymeric side chains,[8] has been also studied in recent years,[9] it remains much less explored in many respects, including morphological control, hierarchical self-assembly, etc.

Herein, we demonstrate a novel type of rod−coil graft copolymer containing an expanded poly-*para*-phenylene backbone grafted with poly(ethylene oxide) (PEO) side chains (Figure 1). Featuring a unique rod−coil structure with a short average distance between neighboring PEO chains on the conjugated backbone, such graft copolymers exhibit remarkable temperature-dependent one-dimensional (1D) and two-dimensional (2D) hierarchical self-assembly behavior in solution above (20 °C) and below (10 °C) the T_c of the PEO chains, respectively. During the 1D self-assembly, the achiral graft copolymers organized into nanoribbons, which further bundled into ultralong helices with controlled pitch depending on the grafting ratio of the PEO chains (Figure 1A). The 2D self-assembly of the graft copolymers resulted in quadrangular multilayer sheets of micrometer-sized lateral dimensions (Figure 1B), for which an unprecedented self-assembly process from nanoribbons to "raft-like" nanostructures and, eventually, to the sheets was observed. To the best of our knowledge, such graft polymers represent the first example of polymers that can selectively self-assemble into 1D helix and 2D sheet superstructures.

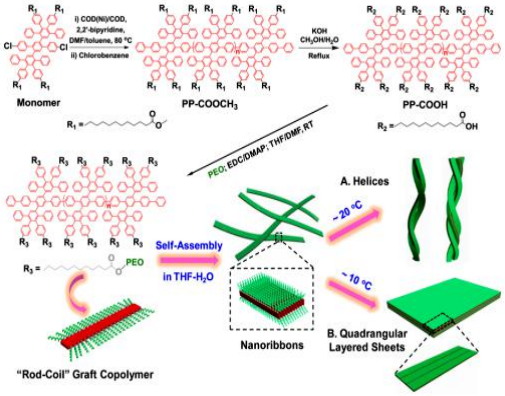

Figure 1. Schematic illustration of the synthesis of rod−coil graft copolymers containing a polyphenylene backbone grafted with PEO side chains as well as the temperature-dependent 1D and 2D hierarchical self-assembly process.

To prepare the rod−coil graft copolymers, laterally expanded poly-*para*-phenylene (i.e., poly-*para*-phenylene with dendritic tetraphenylbenzene substituents) decorated with $C_{10}H_{20}COOCH_3$ (PP-$COOCH_3$) was first synthesized by the

Received: July 17, 2015
Published: September 1, 2015

DOI: 10.1021/jacs.5b07487
J. Am. Chem. Soc. 2015, 137, 11602−11605

Yamamoto polymerization of a dichloro-substituted oligophenylene monomer (Figure 1 and Section 3 in the Supporting Information). After the hydrolysis of PP-$COOCH_3$ to PP-COOH, the graft copolymers were synthesized by the esterification of the carboxyl groups on PP-COOH with the hydroxyl groups at one end of 1K g/mol PEO (Figure 1). The successful grafting of the PEO chains onto the polyphenylene was validated by Fourier transform infrared spectroscopy (FTIR) (Figure S17) and nuclear magnetic resonance (NMR) analyses (Figure S18). Table 1 presents three graft copolymers with

Table 1. NMR and GPC Data for the Graft Copolymers

name	GP (%)[a]	$M_{n,\,calc}$[b]	$M_{n,\,GPC}$[c]	PDI[c]
PP-$COOCH_3$	N/A	N/A	21,400	1.13
GC-91	91	65,100	57,600	1.31
GC-55	55	47,800	42,100	1.27
GC-28	28	34,800	26,000	1.25

[a]PEO grafting percentages measured by NMR. [b]Calculated molecular weights based on M_n (GPC, PP-$COOCH_3$) and GPs. [c]M_n and polydispersity index (PDI) measured by GPC against a polystyrene standard; GPC curves are given in Figures S15 and S19.

different grafting percentages (GPs) of PEO chains, namely, GC-91, GC-55, and GC-28, with GPs of 91%, 55%, and 28%, respectively, as determined by NMR and supported by calculations based on elemental analyses (Pages S16–17). Gel permeation chromatography (GPC) results showed increased number-average molecular weights (M_n) compared with that of PP-$COOCH_3$ (Table 1). The M_n values measured by GPC ($M_{n,\,GPC}$) are slightly smaller than the calculated values ($M_{n,\,calc}$) based on the M_n of PP-$COOCH_3$ and the GPs. This difference is likely caused by the presence of carboxyl groups in the graft polymers, which enhance the adsorption of the polymers on GPC column and thus prolong their exclusion.[10]

The self-assembly of the rod–coil graft copolymers was performed through a cosolvent method[11] at different temperatures by considering the T_c of the tethered PEO chains (see below). Briefly, the copolymers were dissolved in THF, which is a common solvent for both polyphenylene and PEO, to produce a 10^{-3} mg mL^{-1} THF solution; under stirring, the solution was added dropwise (0.06 mL min^{-1}) to a 4-fold amount of pure water, a selective solvent for PEO. The mixed solution turned from colorless to light blue, suggesting the formation of polymer aggregates.

The self-assembly of GC-91 in the THF–water solution at 20 °C generated long helical nanostructures (Figure 2 and Figure S20). The transmission electron microscopy (TEM) samples prepared by freeze-drying gave the same helical structures as those in the vacuum-dried TEM samples, indicating the formation of helices in solution state.[12] Statistics based on 200 helices in the TEM images yielded an average diameter (D) of 44 ± 9 nm (Figure 2A) and lengths of 10–30 μm (up to ~30 μm, Figure S20A,B). Most of the helices comprised two or three ~15 nm wide 1D aggregates (Figure 2B,C); a minority of the helices (<10 number %) was multistranded (≥4 strands) (Figure S20D,E). High-resolution TEM (HRTEM) images revealed a ribbon-like structure of the 1D aggregates of ~15 nm width. For example, Figure 2D presents an HRTEM image of a double-stranded helix with a short untwisted section, in which the "width" of one strand is only ~4 nm, much smaller than that (~15 nm) of the other one. This exceptionally narrow width is attributed to the fact that a 4 nm thick ribbon is located vertically

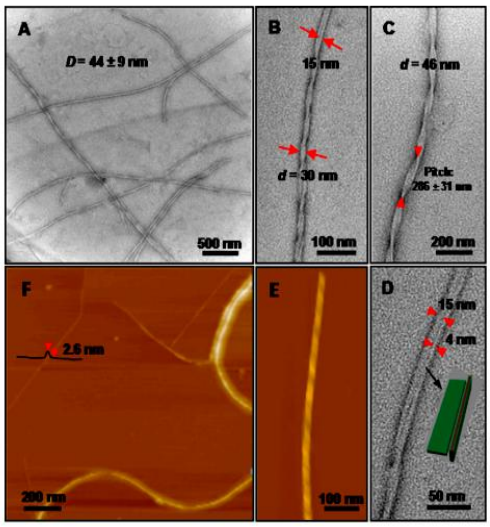

Figure 2. TEM and AFM images of the helices formed by the hierarchical self-assembly of the GC-91 graft copolymers in THF–water (v/v 1:4) at 20 °C. (A) A low-magnification TEM image of the helices (D denotes the average diameter); (B,C) high-magnification TEM images of the double- and triple-stranded helices with related sizes indicated (d expresses a diameter of a specific helix); (D) an HRTEM micrograph of an untwisted region in a double-stranded helix in which a ribbon-like aggregate is positioned vertical to the substrate (inset); (E) an AFM height profile of a helix; and (F) an AFM height image scanned after strong sonication of the helix dispersion in THF–water.

to the substrate under TEM investigation (inset of Figure 2D). As no chiral molecules were used in the self-assembly process, the coexistence of left- and right-handed helices observed by TEM is not surprising. Remarkably, the average diameter and pitch of the helices are tunable by varying the GP of the PEO chains. The statistics indicate that, as the GP of PEO decreases from 91% to 55% and 28%, the average diameter of the resultant helices decreases from 44 ± 9 nm to 39 ± 3 and 32 ± 2 nm, along with a decrease in the average pitch from 286 ± 31 nm to 208 ± 33 and 136 ± 20 nm, respectively (Figure S21).

The helical structure of the GC-91 aggregates was confirmed by atomic force microscopy (AFM) (Figure 2E). To further probe the composition of the helices, we attempted to disassemble the helices by strong sonication of their solutions. AFM profiles manifested that the helices consisted of ribbon-like aggregates with a width of ~15 nm and a thickness of ~2.6 nm (Figure 2F). These two values are very close to the calculated length (~15 nm) and width (~3.9 nm) of a graft copolymer molecule, respectively, suggesting that the ribbon-like aggregates are formed by the parallel alignment of the graft copolymers (see Section 4.3.1, Page S23).

In light of the above-mentioned results, in particular, the dimensions of the graft copolymer molecules and the resultant aggregates, we suggest a possible self-assembly mechanism, as illustrated in Figure 1. Driven by the hydrophobic interaction, the graft copolymers first self-assemble into ~15 nm wide and ~2.6 nm thick nanoribbons with a hydrophobic polyphenylene layer sandwiched by hydrophilic PEO coils. Owing to the relatively low PEO number density at both edges of the nanoribbons, they tend to associate to minimize the polyphenylene–water contact. However, the average distance between adjacent PEO chains in GC-91, GC-55, or GC-28 in the nanoribbons is estimated to be

DOI: 10.1021/jacs.5b07487
J. Am. Chem. Soc. 2015, 137, 11602–11605

~0.7, ~1.2, or ~2.2 nm, respectively (see Section 4.3.2, Pages S24–25). These distances are smaller than twice the radius of gyration (R_g = ~1.5 nm) of a 1K g/mol PEO chain at its end-free state in solution,[13] suggesting the existence of crowded PEO coils around the associated nanoribbons. Thus, the steric interaction among the PEO chains may cause a twist of the associated nanoribbons providing more peripheral space for the PEO coils and lead to the formation of 1D helical superstructures (Figure S22). The peripheral space around a helix within a small pitch can accommodate only a relatively small number of PEO chains; hence, with an increase in the PEO grafting ratio, the pitch of the helices increases accordingly.

Although supramolecular helix formation has been found in a few achiral linear polymers,[3,14] the current study presents the first example of helix formation by achiral graft polymers. More interestingly, we found that the graft copolymers self-organized into free-standing 2D quadrangular multilayer sheets at 10 °C. The sheet formation occurred over a period of days, with the aging of the as-prepared solution of the GC-91 aggregates at 10 °C. Within 5 h of aging, TEM images (Figure 3A) revealed a large number of raft-like assemblies (called "rafts") that consisted of

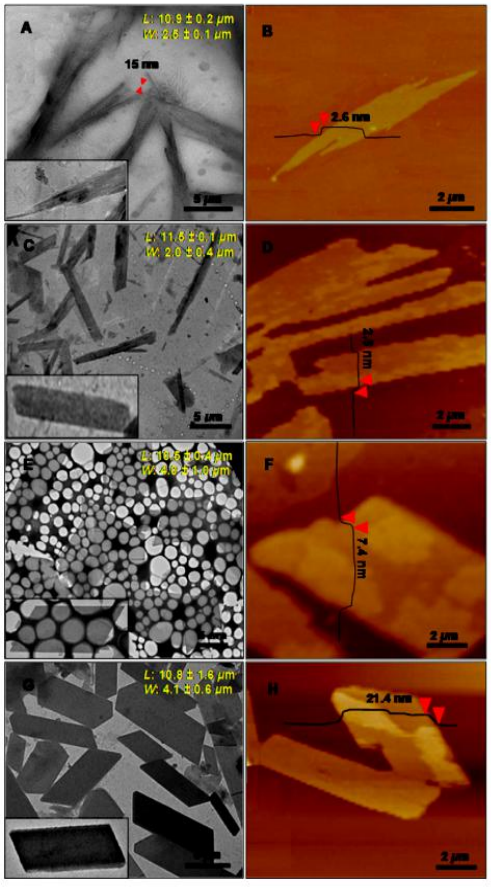

Figure 3. TEM and AFM images of the 2D aggregates formed by the hierarchical self-assembly of GC-91 in THF–water (v/v 1:4) at 10 °C after (A,B) 5 h, (C,D) 1 day, (E,F) 5 days, and (G,H) 10 days. The average lengths (L), widths (W), and thicknesses of the aggregates are indicated in the corresponding TEM and AFM images.

~15 nm wide 1D nanostructures (inset of Figure 3A); the width was similar to that of the above-discussed nanoribbons. Moreover, the thickness of the rafts was ~2.6 nm (Figure 3B), the same as that of the nanoribbons. Therefore, it is reasonable to believe that the rafts are single-layered and formed by the planar alignment of the nanoribbons. Remarkably, with the aging of the solution, the rafts grew to narrow nanosheets (Figure 3C,D) and eventually to quadrangular sheets after ca. 10 days (Figure 3E–H). The thickness of the quadrangular sheets was greater than that of the rafts, suggesting a multilayer feature of the sheets. The quadrangular sheets suspended in solution were also observed by optical microscopy (Figure S23), confirming that the sheets were formed in solution. Moreover, dynamic light scattering (DLS) analyses revealed an obvious increase in the hydrodynamic diameter of the GC-91 assemblies with the aging of the solution at 10 °C, whereas no big change was found in the hydrodynamic size of the GC-91 helices in solution at 20 °C (Figure S24). The results confirm the gradual growth of the GC-91 assemblies in solution at 10 °C.

It is known that PEO crystallization in organic media may contribute to the solution growth of multilayer rhombus crystals of some PEO-containing block copolymers, e.g., PEO-*b*-polycaprolactone in hexanol.[15,16] In the present study, differential scanning calorimetry (DSC) analyses of GC-91 revealed a T_c of ~16 °C for the grafted 1K g/mol PEO chains (Figure S25A). Micro-DSC measurements gave a T_c of ~13 °C for the PEO chains in the GC-91 aggregates in THF–water (Figure S25B). Apparently, the 1D and 2D self-assembly of GC-91 occurred above and below the T_c of the PEO chains, respectively. After GC-91 self-organized into nanoribbons (Figure 1), a short average distance of ~0.7 nm between neighboring PEO chains on the polyphenylene backbone resulted in a high number density of PEO chains at the ribbon surface, which exceeded the onset density for the crystallization of the chains below their T_c (see calculations in Section 4.3.2, Pages S24–25).[16,17] Thus, the crystallization and the resulting compact state of the PEO chains may favor the transformation of the nanoribbons into sheet-like structures.[18] In contrast, the PEO chains at the surfaces of the nanoribbons formed by GC-55 or GC-28 cannot crystallize due to the low density of the chains (Section 4.3.2, Pages S24–25),[16,17] which accounts for the formation of only helices rather than sheets under similar experimental conditions. As the onset density of PEO crystallization is determined by both the dimension of PEO and the average distance between neighboring PEO chains on the polyphenylene, the length of PEO chains, in addition to the GP, can also affect the 2D self-assembly of the graft copolymers. For instance, owning a GP of ~90%, the graft copolymer with 500 g/mol PEO side chains did not form quadrangular multilayer sheets under similar conditions, due to the reduced length of the PEO coils.

To further investigate how the multilayer sheets are related to the crystallization of the PEO chains, the THF–water solution of the sheets was dialyzed against water to remove THF at 10 °C. Interestingly, we found that the multilayer sheets developed into rafts after the removal of the THF (Figure S26A,B). Increasing the temperature of the THF–water solution from 10 to 25 °C also yielded rafts. Such disorganization, the reverse step of the sheet formation, may be caused by the expansion of the PEO coils in solution from a compact crystalline state in the presence of organic media (THF in this case) or below their T_c.[16,18] Moreover, an attempt was made to elucidate the crystal structure of the sheets by electron diffraction (ED). However, no diffraction patterns were observed (Figure S26C), probably

DOI: 10.1021/jacs.5b07487
J. Am. Chem. Soc. 2015, 137, 11602–11605

due to the destruction of the crystal structure at temperatures higher than the T_c of the 1K g/mol PEO upon the irradiation of electron beams.[19]

The optical properties of the GC-91 assemblies in THF–water solutions were studied by ultraviolet–visible (UV–vis) and photoluminescence (PL) spectroscopies (Figure 4). The

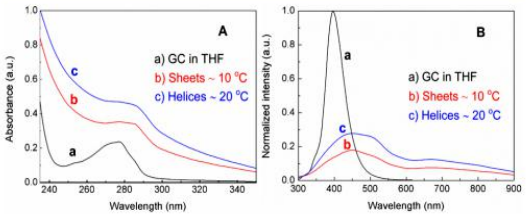

Figure 4. (A) UV–vis and (B) photoluminescence spectra of GC-91 in THF as well as of the helices and the sheets in THF–water (v/v 1:4) at different temperatures (concentration: 2×10^{-4} mg mL^{-1}).

maximum absorption of the helices and the sheets were red-shifted to ~290 nm, compared with 280 nm of GC-91 in THF (Figure 4A), indicative of intermolecular π–π interactions associated with the aggregation of GC-91.[3] The PL spectra revealed a distinct quenching of the photoluminescence of both the helices and the sheets in THF–water (Figure 4B). The PL spectra of the helices remained almost unchanged with the aging of their solution at 20 °C over 10 days, suggesting their good stability in solution;[3] however, the PL spectra of the assemblies obtained at 10 °C showed a consecutive quenching of the photoluminescence (Figure S27), most probably due to the progressive formation of the sheets.

In summary, we prepared a novel type of rod–coil graft copolymer containing a poly-*para*-phenylene backbone grafted with 1K g/mol PEO chains. Remarkably, these polymers performed temperature-dependent 1D and 2D self-assembly in solution. At 20 °C, which is above the T_c of the PEO chains, the achiral graft copolymers self-organized into 1D nanoribbons that further bundled into ~30 μm helices. At 10 °C, which is below the T_c, the self-assembly of the graft copolymers, driven by the crystallization of the tethered PEO chains, resulted in progressive growth of nanoribbons into rafts and eventually into quadrangular multilayer sheets with lateral dimensions of over 10 μm. These novel rod–coil graft polymers provide new opportunities for the controlled preparation of 1D helix and 2D superstructures as well as offer a new system for the fundamental studies on the self-assembly of conjugated polymers, including morphological control, thermodynamics and kinetics, potential applications, etc.

■ ASSOCIATED CONTENT

Supporting Information

The Supporting Information is available free of charge on the ACS Publications website at DOI: 10.1021/jacs.5b07487.

Experiments, supporting figures, and calculations (PDF)

■ AUTHOR INFORMATION

Notes

The authors declare no competing financial interest.

■ ACKNOWLEDGMENTS

The authors thank the financial support from the 973 Programs of China (2012CB933404 and 2013CBA01602), the Natural Science Foundation of China (21320102006 and 21304057), the Natural Science Foundation of Shanghai (13ZR1421200), the Program for Eastern Scholar in Shanghai, and the MPI Partner Group Project for Polymer Chemistry of Graphene Nanoribbons. We also thank the Instrumental Analysis Center of Shanghai Jiao Tong University for some measurements.

■ REFERENCES

(1) (a) Li, C.; Liu, M.; Pschirer, N. G.; Baumgarten, M.; Müllen, K. *Chem. Rev.* **2010**, *110*, 6817. (b) Bonillo, B.; Swager, T. M. *J. Am. Chem. Soc.* **2012**, *134*, 18916. (c) Liu, J.; Li, B.; Tan, Y.; Giannakopoulos, A.; Sanchez-Sanchez, C.; Beljonne, D.; Ruffieux, P.; Fasel, R.; Feng, X.; Müllen, K. *J. Am. Chem. Soc.* **2015**, *137*, 6097.

(2) Jenekhe, S. A.; Chen, X. L. *Science* **1998**, *279*, 1903.

(3) Lee, E.; Hammer, B.; Kim, J.-K.; Page, Z.; Emrick, T.; Hayward, R. C. *J. Am. Chem. Soc.* **2011**, *133*, 10390.

(4) Patra, S. K.; Ahmed, R.; Whittell, G. R.; Lunn, D. J.; Dunphy, E. L.; Winnik, M. A.; Manners, I. *J. Am. Chem. Soc.* **2011**, *133*, 8842.

(5) Zheng, Y.; Zhou, H.; Liu, D.; Floudas, G.; Wagner, M.; Koynov, K.; Mezger, M.; Butt, H.-J.; Ikeda, T. *Angew. Chem., Int. Ed.* **2013**, *52*, 4845.

(6) Liu, N.; Qi, C. G.; Wang, Y.; Liu, D. F.; Yin, J.; Zhu, Y. Y.; Wu, Z. Q. *Macromolecules* **2013**, *46*, 7753.

(7) Kamps, A. C.; Cativo, M. H. M.; Fryd, M.; Park, S.-J. *Macromolecules* **2014**, *47*, 161.

(8) (a) Sheiko, S. S.; Sumerlin, B. S.; Matyjaszewski, K. *Prog. Polym. Sci.* **2008**, *33*, 759. (b) Rzayev, J. *ACS Macro Lett.* **2012**, *1*, 1146.

(9) (a) Yao, J. H.; Mya, K. Y.; Shen, L.; He, B.; Li, L.; Li, Z.; Chen, Z.; Li, X.; Loh, K. P. *Macromolecules* **2008**, *41*, 1438. (b) Lin, J.; Zhu, G.; Zhu, X.; Lin, S.; Nose, T.; Ding, W. *Polymer* **2008**, *49*, 1132. (c) Cai, C.; Lin, J.; Chen, T.; Tian, X. *Langmuir* **2010**, *26*, 2791. (d) Miyake, G. M.; Weitekamp, R. A.; Piunova, V. A.; Grubbs, R. H. *J. Am. Chem. Soc.* **2012**, *134*, 14249.

(10) Turner, S. R.; Walter, F.; Voit, B. I.; Mourey, T. H. *Macromolecules* **1994**, *27*, 1611.

(11) Mai, Y.; Eisenberg, A. *Chem. Soc. Rev.* **2012**, *41*, 5969.

(12) Azzam, T.; Eisenberg, A. *Langmuir* **2010**, *26*, 10513.

(13) The R_g for a PEO chain at its end-free state in solution is estimated using $R_g^2 = b^2 N_b/6$ from Rubenstein, M.; Colby, R. H. *Polymer Physics*; Oxford University Press: New York, 2004, where b = 0.8 nm for PEO.

(14) (a) Zhong, S.; Cui, H.; Chen, Z.; Wooley, K. L.; Pochan, D. J. *Soft Matter* **2008**, *4*, 90. (b) Dupont, J.; Liu, G.; Niihara, K.-I.; Kimoto, R.; Jinnai, H. *Angew. Chem., Int. Ed.* **2009**, *48*, 6144.

(15) Sun, J. R.; Chen, X. S.; He, C. L.; Jing, X. B. *Macromolecules* **2006**, *39*, 3717.

(16) Van Horn, R. M.; Zheng, J. X.; Sun, H.-J.; Hsiao, M.-S.; Zhang, W.-B.; Dong, X.-H.; Xu, J.; Thomas, E. L.; Lotz, B.; Cheng, S. Z. D. *Macromolecules* **2010**, *43*, 6113.

(17) Zheng, J. X.; Xiong, H.; Chen, W. Y.; Lee, K.; Van Horn, R. M.; Quirk, R. P.; Lotz, B.; Thomas, E. L.; Shi, A.-C.; Cheng, S. Z. D. *Macromolecules* **2006**, *39*, 641.

(18) Rizis, G.; van de Ven, T. G. M.; Eisenberg, A. *Angew. Chem., Int. Ed.* **2014**, *53*, 9000.

(19) Egerton, R. F.; Malac, P.; Li, M. *Micron* **2004**, *35*, 399.

JACS
JOURNAL OF THE AMERICAN CHEMICAL SOCIETY

Communication

pubs.acs.org/JACS

Poly(ethylene oxide) Functionalized Graphene Nanoribbons with Excellent Solution Processability

[†]School of Chemistry and Chemical Engineering, Shanghai Jiao Tong University, 800 Dongchuan RD, Shanghai 200240, China
[‡]Max Planck Institute for Polymer Research, Ackermannweg 10, 55128 Mainz, Germany
[§]Division of Molecular Imaging and Photonics, Department of Chemistry, KU Leuven Celestijnenlaan, 200 F, B-3001 Leuven, Belgium
[∥]Interdisciplinary Nanoscience Center, Aarhus University, Gustav Wieds Vej 14, DK-8000 Aarhus C, Denmark
[⊥]Institute of Physical Chemistry, Westfälische Wilhelms-Universität Münster, Corrensstr. 28/30, D-48149 Münster, Germany
[#]School of Chemistry, Manchester University, Oxford Road, Manchester M139PL, United Kingdom
[▽]Institute of Physics, Chinese Academy of Sciences, P.O. Box 603, Beijing 100190, China
[◆]Department of Chemistry and Food Chemistry, Technische Universität Dresden, Mommsenstrasse 4, 01062 Dresden, Germany

Supporting Information

ABSTRACT: Structurally well-defined graphene nanoribbons (GNRs) have attracted great interest as next-generation semiconductor materials. The functionalization of GNRs with polymeric side chains, which can widely broaden GNR-related studies on physiochemical properties and potential applications, has remained unexplored. Here, we demonstrate the bottom-up solution synthesis of defect-free GNRs grafted with flexible poly(ethylene oxide) (PEO) chains. The GNR backbones possess an armchair edge structure with a width of 1.0−1.7 nm and mean lengths of 15−60 nm, enabling near-infrared absorption and a low bandgap of 1.3 eV. Remarkably, the PEO grafting renders the GNRs superb dispersibility in common organic solvents, with a record concentration of ∼1 mg mL^{-1} (for GNR backbone) that is much higher than that (<0.01 mg mL^{-1}) of reported GNRs. Moreover, the PEO-functionalized GNRs can be readily dispersed in water, accompanying with supramolecular helical nanowire formation. Scanning probe microscopy reveals raft-like self-assembled monolayers of uniform GNRs on graphite substrates. Thin-film-based field-effect transistors (FETs) of the GNRs exhibit a high carrier mobility of ∼0.3 cm^2 V^{-1} s^{-1}, manifesting promising application of the polymer-functionalized GNRs in electronic devices.

Graphene nanoribbons (GNRs) have attracted great attention as candidates for next-generation semiconductor materials.[1−3] Their electronic properties, such as the finite bandgap, are strongly governed by their width and edge structures. Among a number of "top-down"[1,4,5] and "bottom-up"[2,6−10] approaches developed for the fabrication of GNRs, bottom-up solution synthesis shows an incomparable advantage in large-scale production of liquid-phase-processable GNRs with well-defined structures.[2,6,7] Nevertheless, chemically synthesized GNRs either have no side substituents or are functionalized only with short alkyl chains,[2,7,11,12] which greatly limits their solution processability and thus impedes their deeper fundamental studies and prospective applications. Attachment of polymer chains to GNR backbones would offer a promising strategy to surmount this barrier. This approach, however, has remained unexplored.

Here, we demonstrate the bottom-up solution synthesis of GNRs grafted with flexible poly(ethylene oxide) (PEO) chains, which involves the pre-introduction of methoxycarbonyl and carboxylic active groups on the periphery of GNRs (Scheme 1). The PEO-functionalized GNRs (GNR-PEO) have a PEO grafting percentage (GP) of 46% and shows excellent dispersibility in common organic solvents such as tetrahydrofuran (THF), with high concentrations of up to ∼1 mg mL^{-1} (for the GNR backbone), superior to those of reported GNRs (<0.01

Scheme 1. Synthetic Route Towards PEO-Functionalized GNRs

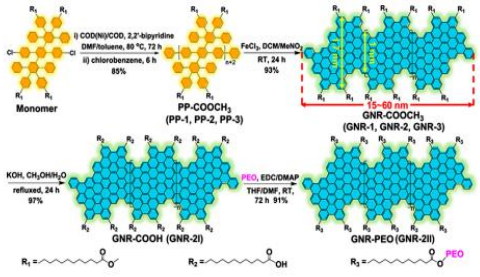

Received: July 8, 2016
Published: July 27, 2016

DOI: 10.1021/jacs.6b07061
J. Am. Chem. Soc. 2016, 138, 10136−10139

mg mL^{-1}).[2,3] UV−vis studies of GNR-PEO in THF revealed a near-infrared (NIR) absorption with the maximum at ~650 nm and an optical bandgap of ~1.3 eV. Interestingly, GNR-PEO was water-dispersible, exhibiting red-shifted absorption bands, which are associated with the formation of helical nanowire superstructure of the GNRs. Photoluminescence (PL) spectrometry unveiled NIR emission with the maximum at ~920 nm for GNR-PEO in THF, while complete PL quenching was detected for the GNRs in aqueous solution. Scanning probe microscopy (SPM) analysis of GNR-PEO deposited on graphite substrates revealed a raft-like ordered self-assembled monolayer structure. The excellent solution processability of GNR-PEO allowed the fabrication of thin-film-based field-effect transistors (FETs) by directly drop-casting their THF dispersions on Si/SiO_2 substrates, exhibiting a high carrier mobility of ~0.3 cm^2 V^{-1} s^{-1}, which is superior to those of GNR thin-film based FETs reported previously.[13,14]

The chemical synthesis toward GNR-PEO is illustrated in Scheme 1, and the detailed procedures are described in the Supporting Information (SI). First, laterally expanded poly-*para*-phenylene decorated with $-C_{10}H_{20}COOCH_3$ chains (named as PP-$COOCH_3$) was prepared by AA-type Yamamoto polymerization of a dichloro-substituted oligophenylene monomer.[15] The successful synthesis of PP-$COOCH_3$ was demonstrated by nuclear magnetic resonance (NMR) and gel permeation chromatography (GPC) studies (Figures S1−S3).[15] GPC analyses against polystyrene standard revealed that the PP-$COOCH_3$ samples had different number-average molecular weights (M_ns) ranging from 20,000 to 80,000 as well as narrow polydispersity indices (PDI) of 1.06−1.12 (PP-1, PP-2, and PP-3 in Table 1). Second, the PP-$COOCH_3$ samples were transformed into GNRs with a *para*-armchair edge structure as well as a width of 1.0−1.7 nm and different calculated average lengths of 15−60 nm (Scheme 1 and Table 1), by employing intramolecular cyclodehydrogenation in CH_2Cl_2 solution using $FeCl_3$ as the Lewis acid and oxidant.[7] As PP-2 with the M_n of ~40,000 was easier to obtain by the Yamamoto polymerization in the present study, the synthesis of GNR-2 with a mean length of ~30 nm could be readily scaled up to the gram scale. Third, the hydrolysis of GNR-2 yielded GNR-COOH, where the carboxyl groups afforded opportunities for further modification of the GNRs. Finally, GNR-PEO with a PEO grafting percentage of 46% was achieved by the esterification of the carboxyl groups in GNR-COOH with the hydroxyl groups at one end of 1 kg/mol PEO chains (Scheme 1).

Table 1. GPC Data of PP-$COOCH_3$ Samples and Lengths of the Corresponding GNRs

PP-$COOCH_3$	M_n (g/mol)	PDI	GNR-$COOCH_3$	GNR-COOH	GNR-PEO	GNR length (nm)[a]
PP-1	19,900	1.06	GNR-1	–	–	~15
PP-2	42,300	1.12	GNR-2	GNR-2I	GNR-2II	~30
PP-3	82,100	1.10	GNR-3	–	–	~60

[a]The lengths are calculated based on M_n of the polyphenylene precursors

Fourier transform infrared (FTIR) analyses reveal significant attenuation of the signals from aromatic C−H stretching vibrations at 3083, 3050, and 3024 cm^{-1} as well as the out-of-plane (*opla*) C−H deformation bands at 829, 809, and 698 cm^{-1} in the spectrum of GNR-$COOCH_3$ compared with that of PP-$COOCH_3$ (Figures S10−12).[7,16,17] In addition, typical *opla* bands for aromatic C−H at the armchair edge of the GNR basal plane appear at 816 and 861 cm^{-1}.[7,18] These results validate the efficient "graphitization" of the polyphenylene backbone into GNR.[2,7] The FTIR spectrum of GNR-PEO (Figure S14) shows a distinct increase in intensity of the band at 1730 cm^{-1} (the stretching of C═O in ester group) and an attenuation of the signal at 1702 cm^{-1} (the stretching of C═O in carboxyl group), demonstrating the successful grafting of the PEO chains. The ^{13}C solid-state NMR analysis reveals a grafting percentage of 46% for GNR-PEO, which is supported by the calculation based on thermogravimetric analysis (Figures S15−16 and pp S18−19, SI). Moreover, solid-state ^{1}H NMR spectroscopy reveals that PP-$COOCH_3$, with a semiflexible to semirigid structure, becomes rigid and planar after graphitization into GNR (Figure S17).[2,3] Specifically, the 2D ^{1}H−^{1}H double quantum−single quantum (DQ-SQ) correlation spectra show broad, stretched, and split ridge signals in the aromatic regions (Figure S17), which originate from the interactions between the two types of aromatic protons at the edge of the GNRs, confirming the graphitization of PP-$COOCH_3$.[2,3]

The Raman spectra of the resulting GNRs exhibit typical D and G peaks (Figures 1a and S18), as reported for other GNRs.[2,7,19] Figure 1a shows that the first-order Raman spectrum is not strongly dependent on the functionalization of the GNRs. Importantly, a distinct peak, associated with the radial breathing-like mode (RBLM),[2,8] is observed at ~170 cm^{-1} for all GNR samples. The presence of this peak confirms the atomically precise and low-dimensional structure of GNRs.[2,19] By using the relation: $w = 3222/\nu_{RBLM}$ Å, where w is the width and ν_{RBLM} is the RBLM wavenumber,[2,3] the mean width of our GNRs is experimentally estimated to be ~1.9 nm, which is in good agreement with the calculated value of 1.7 nm (Scheme 1). The RLBM of these GNRs seems to be less affected by the edge pattern geometry, compared to other GNRs, where a strong discrepancy between experimental and calculated RLBM position has been observed.[19]

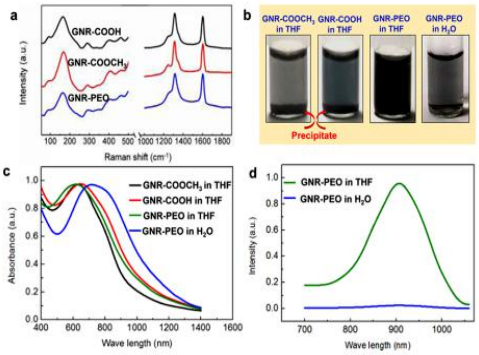

Figure 1. (a) Raman spectra of the GNRs with identical mean lengths of ~30 nm (excited at 638 nm). (b) Photos of GNR dispersions in THF (1.0 mg mL^{-1} for GNR backbone) and in H_2O (0.2 mg mL^{-1}) after sonication for 5 min. (c) UV−vis spectra of GNR dispersions (0.01 mg mL^{-1}). (d) PL spectra of CNR-PEO dispersions (0.01 mg mL^{-1}).

Owing to the high-degree grafting of PEO chains, the resultant GNRs exhibit superior dispersibility in conventional organic solvents including THF, chloroform, chlorobenzene, and 1,2,4-trichlorobenzene (TCB), etc. Mild sonication of GNR-PEO in these organic solvents, e.g., in THF, generated black homoge-

DOI: 10.1021/jacs.6b07061
J. Am. Chem. Soc. 2016, 138, 10136−10139

neous dispersions with high concentrations up to ~1 mg mL^{-1} (for GNR backbone, Figure 1b). The dispersions were stable without visual precipitation for at least 1 day. In sharp contrast, GNR-$COOCH_3$ and GNR-COOH could not be homogeneously dispersed in these solvents under similar experimental conditions, and a visible precipitate was observed within several minutes after sonication (Figure 1b). The highest concentrations of GNR-$COOCH_3$ and GNR-COOH in THF only reached ~0.02 and ~0.05 mg mL^{-1}, respectively (Figure S20). Moreover, the dispersibility of GNR-PEO is much better than that of reported alkylated GNRs (<0.01 mg mL^{-1} in dispersions).[2,3] On the other hand, dynamic light scattering (DLS) analysis gave a single narrow size distribution with an average hydrodynamic diameter (D_h) of ~40 nm for GNR-PEO in THF (Figure S21). The fact that the mean D_h is close to the calculated size (~30 nm) of a single PEO-modified GNR suggests the lack of serious aggregation of GNR-PEO in THF. This result contrasts starkly to those from reported alkylated GNRs, which suffer from pronounced aggregation under similar conditions.[2,3]

Remarkably, GNR-PEO was also water-dispersible with a high concentration of ~0.2 mg mL^{-1} of the GNR backbone (Figure 1b). The dispersions were stable for several hours depending on the concentration. DLS study gave a much increased mean D_h (~450 nm) for GNR-PEO in H_2O, suggesting supramolecular assembly of the GNRs (Figure S21). Transmission electron microscopy and AFM revealed an interesting helical nanowire superstructure for the GNR assemblies, which has a mean diameter of 25 ± 12 nm, lengths of 5−20 μm and an average pitch of 48 nm (Figure S22).

The excellent dispersibility of GNR-PEO in common solvents offers opportunities for a wide range of solution-based physical characterizations. UV−vis spectrum of GNR-PEO in a dilute THF dispersion reveals NIR absorption with the maximum at ~650 nm and an optical bandgap of ~1.3 eV (Figure 1c). This bandgap agrees well with the calculated value of 1.34 eV for *para*-armchair edge GNRs based on density functional theory.[20] The absorption spectra of GNR-$COOCH_3$ and GNR-COOH in THF display similar features to that of GNR-PEO (Figure 1c). In contrast, GNR-PEO in H_2O exhibits a significantly red-shifted main absorption band associated with a lower bandgap of ~1.0 eV (Figure 1d). On the other hand, the GNRs with different mean lengths of 15−60 nm exhibit an identical bandgap of 1.3 eV (Figure S23), suggesting negligible longitudinal confinement in determining the bandgaps of GNRs of over 15 nm in length. As serious aggregation generally quenches the fluorescence of GNRs, their PL characteristics have been difficult to obtain. In our work, GNR-PEO in dilute THF dispersion gave a PL spectrum with the emission maximum at ~920 nm (Figure 1d), attributable to the outstanding dispersibility of GNR-PEO. In contrast, GNR-PEO in H_2O shows complete PL quenching due to the strong aggregation of the GNRs.

Self-assembled monolayers of GNR-PEO were investigated at the liquid−solid interface by means of scanning tunnel microscopy (STM). Figure 2a displays a typical STM image of GNR-PEO deposited on highly oriented pyrolytic graphite (HOPG) using hot TCB, which reveals small domains of self-assembled GNRs where individual GNRs are coaligned side by side into a lamellar structure. The average longitudinal size (>100 nm) of the lamellae is larger than the length of a single GNR, indicating an end-to-end alignment of the GNRs within a lamella. The periodicity of these stripes is in the range of 5.1−5.7 nm, much lower than the width of a GNR-PEO with fully extended side-chains. This suggests that the PEO chains either form

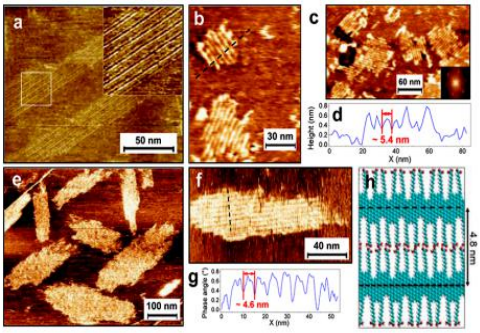

Figure 2. (a) STM image of isolated GNR-PEO domains at the TCB/HOPG interface (I_{set} = 100 *p*A, V_{bias} = −0.6 V). (b, c) AFM topography images of self-assembled GNR-PEO monolayers on HOPG upon drying. Inset in (c) shows a Fourier transform of the image showing the three axes of the 5.4 nm wide lamellas. (d) Line profile along the black dotted line in the AFM image in panel (b) shows the formation of a monolayer film. (e, f) AFM phase images of isolated GNR-COOH domains on HOPG upon drying. (g) Line profile along the black dotted line in panel (f) shows a periodicity of 4.6 nm for the lamellae. (h) A molecular model depicting the plausible arrangement of GNR-COOH in the organized monolayers. In this model, alkyl chains are fully extended and adjacent molecules possibly interact with each other via hydrogen bonding of the terminal carboxyl groups; the GNRs parallel to each other without stacking or interdigitation of the alkyl chains. The periodicity is 4.8 nm.

coiled/entangled bundles between the aromatic backbones of adjacent GNRs or are back-folded in the supernatant solution. Similar behavior was reported earlier where oligoethylene oxide chains remain in solution due to their lower adsorption energy on graphite compared with alkyl chains.[21] Besides, the lamellae appear as a repetition of double bright stripes sandwiching a dark one, which could be induced by the introduction of the PEO chains. Lamellae of various sizes (tens of nm) on HOPG were also imaged by atomic force microscopy (AFM) after evaporation of the solvent (Figure S25), including assemblies of only a few GNRs and even stripes compatible with single GNRs (Figure 2b,c). A line profile traced on the AFM image shows a height difference of ~0.4 nm between graphite and the GNRs (Figure 2d), validating the formation of organized monolayers. The average periodicity of the stripes in the lamellae is 5.4 ± 0.3 nm, in agreement with the result from STM.

In comparison, AFM analysis of GNR-COOH dry films on HOPG revealed similar monolayer structures with striped domains (Figure 2e,f). The mean periodicity of the stripes in a GNR-COOH lamella is 4.6 ± 0.2 nm (Figure 2g), which is in accordance with the calculated assembly model of GNR-COOH (periodicity: 4.8 nm, Figure 2h). The 0.8 ± 0.5 nm difference in periodicity between the two types of GNRs can be explained by the insertion of PEO "rows" in the lamellae, the interactions of which allows the organization of GNR-PEO into a regular pattern.

Profiting from the excellent dispersibility of GNR-PEO in common organic solvents, we investigated the electronic properties of the GNRs by fabricating GNR-based thin-film FETs. To this end, GNR-PEO was deposited between Ti/Au electrodes on Si/SiO_2 substrate by drop-casting of the dispersion (0.5 mg mL^{-1}) in THF (Figure S27A). The subsequent mild heating vaporized THF rapidly and left a GNR thin film behind without solvent contamination, which is a great advantage of low-boiling solvents. Afterward, the substrate was annealed under a

DOI: 10.1021/jacs.6b07061
J. Am. Chem. Soc. 2016, 138, 10136−10139

H_2/Ar atmosphere at 500 °C, which is an optimum temperature to cut off the insulating alkyl chains from GNRs to reduce ribbon-to-ribbon junction resistance without affecting the GNR basal plane.[13] FTIR and Raman spectroscopies of the film revealed no apparent influence of the thermal treatment on the GNR backbone (Figure S28A,B). Moreover, the GNR thin film between two Ti/Au electrodes was imaged by SEM and AFM, which gave a length of ~3 μm, a width of ~3 μm, and a thickness of ~27 nm for the film (Figures S27B and S28C). In contrast, GNR-$COOCH_3$ and GNR-COOH could only form discontinuous films with massive aggregates on the substrate under the similar drop-casting conditions, attributable to their much poorer dispersibility in THF.

The current vs drain voltage (I–V_d) and current vs gate voltage (I–V_{gs}) for the channel length $L \sim 3$ μm thin-film FET are displayed in Figure S27C,D. The I–V_d curves of the thin film before and after annealing at 500 °C prove that annealing can significantly increase the conduction (inset in Figure S27C). The thin-film FET exhibited maximum carrier mobility of ~0.3 cm^2 V^{-1} s^{-1} and an on–off ratio of ~4 under a low voltage of 20 V (Figure S27D, the calculation is provided in the SI, p S29). Although the GNR thin film still revealed a limited p-type current modulation, which is probably due to the electric-field screening effect in GNR films and relatively high ribbon-to-ribbon junction resistance,[22,23] the resultant mobility represents the best among those of GNR-thin-film based FETs reported thus far.[13,14]

In summary, we demonstrated the first bottom-up solution synthesis of polymer-functionalized GNRs with defined structures. The resultant GNR-PEO exhibited an outstanding dispersibility in common organic solvents and even water. The excellent dispersibility offers opportunities not only for deep understanding physiochemical properties of GNRs by a wide range of solution-based physical characterizations including UV–vis, PL, DLS, and SPM, etc., but also for developing prospective applications such as GNR-thin-film based FETs. This study blazes a trail for polymer functionalization of GNRs, which holds promise to prepare thin films with controlled alignment of GNRs by solution deposition. This means might enhance the electrical properties of bottom-up synthesized GNRs. Moreover, polymer functionalization affords chances to develop new GNR-related studies in a broad range of research areas including molecular self-assembly, nanocomposites, and biotechnology, etc.

■ ASSOCIATED CONTENT

Supporting Information

The Supporting Information is available free of charge on the ACS Publications website at DOI: 10.1021/jacs.6b07061.

Experiment details and data (PDF)

■ AUTHOR INFORMATION

■ ACKNOWLEDGMENTS

This work was financially supported by the 973 Programs of China (2013CBA01602), the Natural Science Foundation of China (21320102006, 21304057, and 51573091), the MPI Partner Group Project for Polymer Chemistry of GNRs, EC under Graphene Flagship (no. CNECT-ICT-604391), the European Union's Seventh Framework Programme (FP7/2007-2013)/ERC grant (no. 340324), and the Villum Foundation under the Young Investigator Programme (VKR023122). The authors also thank the Center for Advancing Electronics Dresden (CFAED) and the Instrumental Analysis Center of Shanghai Jiao Tong University for some measurements.

■ REFERENCES

(1) Wang, X.; Dai, H. *Nat. Chem.* **2010**, *2*, 661.
(2) Narita, A.; Feng, X.; Hernandez, Y.; Jensen, S. A.; Bonn, M.; Yang, H.; Verzhbitskiy, I. A.; Casiraghi, C.; Hansen, M. R.; Koch, A. H. R.; Fytas, G.; Ivasenko, O.; Li, B.; Mali, K. S.; Balandina, T.; Mahesh, S.; De Feyter, S.; Müllen, K. *Nat. Chem.* **2013**, *6*, 126.
(3) Narita, A.; Verzhbitskiy, I. A.; Frederickx, W.; Mali, K. S.; Jensen, S. A.; Hansen, M. R.; Bonn, M.; De Feyter, S.; Casiraghi, C.; Feng, X.; Müllen, K. *ACS Nano* **2014**, *8*, 11622.
(4) Li, X.; Wang, X.; Zhang, L.; Dai, H. *Science* **2008**, *319*, 1229.
(5) Kosynkin, D. V.; Higginbotham, A. L.; Sinitskii, A.; Lomeda, J. R.; Dimiev, A.; Price, B. K.; Tour, J. M. *Nature* **2009**, *458*, 872.
(6) Yang, X.; Dou, X.; Rouhanipour, A.; Zhi, L.; Müllen, K. *J. Am. Chem. Soc.* **2008**, *130*, 4216.
(7) Schwab, M.; Narita, A.; Hernandez, Y.; Balandina, T.; Mali, K. S.; De Feyter, S.; Feng, X.; Müllen, K. *J. Am. Chem. Soc.* **2012**, *134*, 18169.
(8) Cai, J.; Ruffieux, P.; Jaafar, R.; Bieri, M.; Braun, T.; Blankenburg, S.; Muoth, M.; Seitsonen, A. P.; Saleh, M.; Feng, X.; Müllen, K.; Fasel, R. *Nature* **2010**, *466*, 470.
(9) Cai, J.; Pignedoli, C. A.; Feng, X.; Müllen, K.; Fasel, R. *Nat. Nanotechnol.* **2014**, *9*, 896.
(10) Ruffieux, P.; Wang, S.; Yang, B.; Sánchez-Sánchez, C.; Liu, J.; Dienel, T.; Talirz, L.; Shinde, P.; Pignedoli, C. A.; Passerone, D.; Dumslaff, T.; Feng, X.; Müllen, K.; Fasel, R. *Nature* **2016**, *531*, 489.
(11) Vo, T. H.; Shekhirev, M.; Kunkel, D. A.; Morton, M. D.; Berglund, E.; Kong, L.; Wilson, P. M.; Dowben, P. A.; Enders, A.; Sinitskii, A. *Nat. Commun.* **2014**, *5*, 3189.
(12) Vo, T. H.; Shekhirev, M.; Kunkel, D. A.; Orange, F.; Guinel, M. J.-F.; Enders, A.; Sinitskii, A. *Chem. Commun.* **2014**, *50*, 4172.
(13) Abbas, A. N.; Liu, G.; Narita, A.; Orosco, M.; Feng, X.; Müllen, K.; Zhou, C. *J. Am. Chem. Soc.* **2014**, *136*, 7555.
(14) Gao, J.; Uribe-Romo, F. J.; Saathoff, J. D.; Arslan, H.; Crick, C. R.; Hein, S. J.; Itin, B.; Clancy, P.; Dichtel, W. R.; Loo, Y. L. *ACS Nano* **2016**, *10*, 4847.
(15) Huang, Y.; Mai, Y.; Yang, X.; Beser, U.; Liu, J.; Zhang, F.; Yan, D.; Müllen, K.; Feng, X. *J. Am. Chem. Soc.* **2015**, *137*, 11602.
(16) Centrone, A.; Brambilla, L.; Renouard, T.; Gherghel, L.; Mathis, C.; Müllen, K.; Zerbi, G. *Carbon* **2005**, *43*, 1593.
(17) Shifrina, Z. B.; Averina, M. S.; Rusanov, A. L.; Wagner, M.; Müllen, K. *Macromolecules* **2000**, *33*, 3525.
(18) Wu, J. S.; Gherghel, J.; Watson, M. D.; Li, J.; Wang, Z.; Simpson, C. D.; Kolb, U.; Müllen, K. *Macromolecules* **2003**, *36*, 7082.
(19) Verzhbitskiy, I. A.; Corato, M. D.; Ruini, A.; Molinari, E.; Narita, A.; Schwab, M. G.; Bruna, M.; Yoon, D.; Milana, S.; Feng, X.; Müllen, K.; Ferrari, A. C.; Casiraghi, C.; Prezzi, D. *Nano Lett.* **2016**, *16*, 3442.
(20) Osella, S.; Narita, A.; Schwab, M. G.; Hernandez, Y.; Feng, X.; Müllen, K.; Beljonne, D. *ACS Nano* **2012**, *6*, 5539.
(21) Chen, L.; Mali, K. S.; Puniredd, S. R.; Baumgarten, M.; Parvez, K.; Pisula, W.; De Feyter, S.; Müllen, K. *J. Am. Chem. Soc.* **2013**, *135*, 13531.
(22) Do, J. W.; Estrada, D.; Xie, X.; Chang, N. N.; Mallek, J.; Girolami, G. S.; Rogers, J. A.; Pop, E.; Lyding, J. W. *Nano Lett.* **2013**, *13*, 5844.
(23) Sangwan, V. K.; Ortiz, R. P.; Alaboson, J. M.; Emery, J. D.; Bedzyk, M. J.; Lauhon, L. J.; Marks, T. J.; Hersam, M. C. *ACS Nano* **2012**, *6*, 7480.

DOI: 10.1021/jacs.6b07061
J. Am. Chem. Soc. 2016, 138, 10136–10139

Polymer Chemistry

COMMUNICATION

View Article Online
View Journal | View Issue

Ultra-large sheet formation by 1D to 2D hierarchical self-assembly of a "rod–coil" graft copolymer with a polyphenylene backbone†

Cite this: *Polym. Chem.*, 2016, **7**, 1234

Received 10th December 2015,
Accepted 4th January 2016

DOI: 10.1039/c5py01969a

www.rsc.org/polymers

This communication reports a unique ultra-large sheet formation through hierarchical self-assembly of a rod–coil graft copolymer containing a rigid polyphenylene backbone and flexible poly(ethylene oxide) (PEO) side chains. The hierarchical self-assembly process involved a distinctive morphological transition of 1D helical to 2D superstructures. The graft copolymer offers a new chance for the challenging bottom-up fabrication of ultra-large self-assembled nanosheets in solution, as well as a novel system for fundamental studies on 2D self-assembly of polymers.

"Rod–coil" graft copolymers are an important type of polymer containing a rigid backbone with densely tethered flexible polymeric chains.[1–3] Their interesting one-dimensional (1D) brush-like structure leads to numerous potential applications, such as molecular actuators, templates for metal nanowires, *etc*.[1,3] Conjugated polymers, *e.g.* polyphenylene and polythiophene, are the major category of rigid backbones in rod–coil graft copolymers, as introducing pendant moieties onto conjugated polymers to form graft copolymers is a general pathway to improve their solubility and tailor their optoelectronic properties.[4–6]

Self-assembly of rod–coil graft copolymers with conjugated polymer backbones and their linear counterpart, rod–coil block copolymers, has attracted much attention in recent decades, as rod–coil copolymers show distinct self-assembly features compared with flexible (coil–coil) copolymer systems due to the introduction of rigid blocks;[6–20] moreover, the resultant supermolecular nanostructures of conjugated polymers generally exhibit unique thermal, optical or optoelectronic properties.[6–20] In particular, the self-assembly of the rod–coil block copolymers has been studied extensively. Several key issues, including aggregate morphologies, morphological control approaches, *etc*., have been explored.[7–16] For example, Winnik, Manners and coworkers prepared nanocylinders of controlled lengths by the crystallization-driven self-assembly of poly(3-hexylthiophene)-*block*-poly-(dimethylsiloxane) rod–coil block copolymers.[8] Although the self-assembly of rod–coil graft copolymers has also been investigated in recent years,[6,17–20] it remains much less understood compared with that of rod–coil block copolymers.

In the present study, we synthesized a rod–coil graft copolymer containing a laterally expanded poly-*para*-phenylene backbone (*i.e.* poly-*para*-phenylene with dendritic tetraphenylbenzene substituents) tethered with poly(ethylene oxide) (PEO) side chains. Interestingly, the graft copolymer exhibited hierarchical self-assembly behavior in a $CHCl_3$–CH_3OH organic cosolvent at room temperature (Fig. 1). Driven by the methanolphobic interaction of the polyphenylene and the crystallization of the PEO chains, the graft copolymer first self-organized into 1D nanowires, which bundled into 10–60 μm ultralong helices, then evolved to 2D raft-like nanostructures, and, eventually, to ultra-large multilayered nanosheets with remarkable lateral dimensions of *ca.* 10 μm × 10 μm to 100 μm × 100 μm, after the aging of the aggregate solution for *ca.* 2 days (Fig. 1). To the best of our knowledge, the bottom-up preparation of such large polymeric sheets by supramolecular self-assembly, without support from a planar interface, has been a severe challenge with only a few successful cases[21,22] and has not been achieved for graft copolymers before, as planar polymer assemblies usually rolled or closed and formed tubes or vesicles in solution.[23] In addition, the unprecedented hierarchical self-assembly process involving 1D helical to 2D superstructures provides a significant reference for the 2D self-assembly of polymers.

The synthesis procedure of the rod–coil graft copolymer is illustrated in Scheme S1† and the experimental details are described in the ESI.† First, Yamamoto polymerization of a dichloro-substituted oligophenylene monomer produced a laterally expanded poly-*para*-phenylene modified with $-C_{10}H_{20}COOCH_3$ (denoted as PP-$COOCH_3$). Then, PP-$COOCH_3$ was hydrolyzed to PP-COOH. Afterwards, the esterification of

[a]*School of Chemistry and Chemical Engineering, Shanghai Jiao Tong University, 800 Dongchuan RD, Shanghai 200240, P. R. China. E-mail: mai@sjtu.edu.cn*
[b]*Department of Chemistry and Food Chemistry, Technische Universität Dresden, Mommsenstrasse 4, 01062 Dresden, Germany*

†Electronic supplementary information (ESI) available: Experimental details, ESI figures, calculations, *etc*. See DOI: 10.1039/c5py01969a

‡These authors contributed equally.

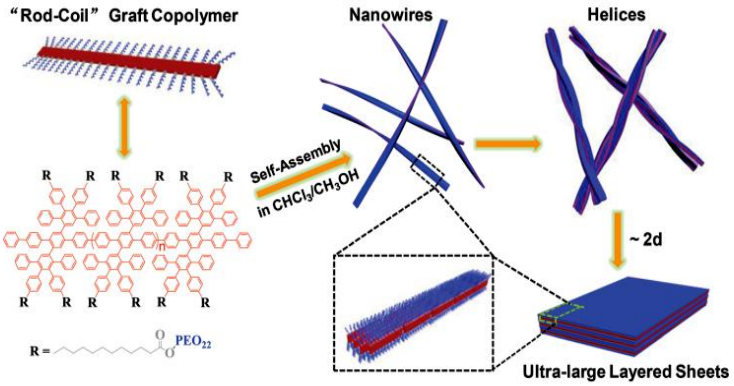

Fig. 1 Schematic illustration of the formation of ultra-large multilayered sheets by 1D to 2D hierarchical self-assembly of the rod–coil graft copolymer at room temperature.

the carboxyl groups on PP-COOH with the hydroxyl groups on 1 kg mol^{-1} poly(ethylene oxide) monomethyl ether yielded the graft copolymer. Fourier transform infrared (FTIR) spectroscopy (Fig. S4A†) and nuclear magnetic resonance (NMR) (Fig. S5†) measurements validated the successful grafting of the PEO chains.

The grafting percentage (GP) of the copolymer was determined to be ~92% by NMR, which was supported by the calculation based on elemental analyses (EA) (see pages S8 and S9†). Gel permeation chromatography (GPC) analysis against polystyrene standards in tetrahydrofuran (THF) gave a number-average molecular weight (M_n) of 136 200 g mol^{-1} and a polydispersity index (PDI) of 1.3 for the graft copolymer, as well as a M_n of 51 700 g mol^{-1} and a PDI of 1.1 for PP-$COOCH_3$ (their single-peak distribution GPC curves are presented in Fig. S4B†). The much larger M_n of the graft copolymer further confirmed the successful grafting of the PEO coils.

The self-assembly of the rod–coil graft copolymer was carried out through a cosolvent method[23] at room temperature (~20 °C). First, a $CHCl_3$ solution with a concentration of 0.01 mg mL^{-1} was prepared by dissolving the graft copolymer in $CHCl_3$, which is a common solvent for both polyphenylene and PEO. Then, under gentle stirring, the $CHCl_3$ solution was added dropwise (~60 μL min^{-1}) into a 9-fold amount of CH_3OH, a selective solvent for PEO. Finally, a light blue mixed solution was obtained, suggesting the formation of polymer aggregates. The as-prepared solution was incubated at room temperature for a period of days.

The aggregation of the graft copolymer in the $CHCl_3$–CH_3OH (v/v 1 : 9) cosolvent was confirmed by ultraviolet-visible (UV-vis) and photoluminescence (PL) spectroscopy (Fig. 2). The maximum absorption of the copolymer in $CHCl_3$–CH_3OH red-shifted to ~280 nm compared with ~270 nm in $CHCl_3$ (Fig. 2A), indicating π–π interactions associated with the aggregation of the polyphenylene backbones.[9] The PL spectra showed the distinct quenching of the photoluminescence of the copolymer in $CHCl_3$–CH_3OH (Fig. 2B), further confirming polymer aggregation. In addition, the consecutive quenching

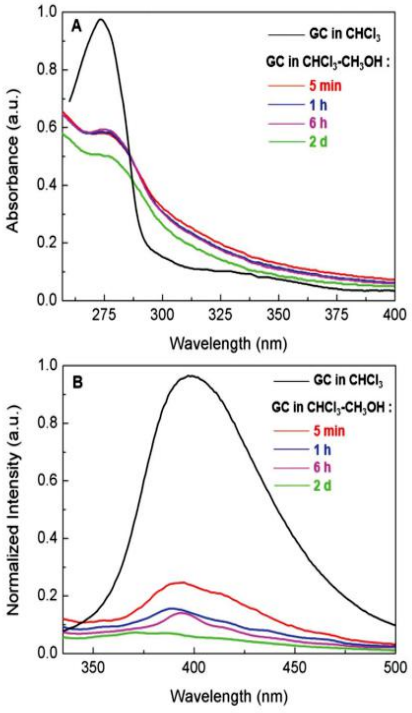

Fig. 2 (A) UV-Vis and (B) photoluminescence spectra of the graft copolymer (GC) in $CHCl_3$ and in $CHCl_3$–CH_3OH (v/v 1 : 9) with the aging (from 5 minutes to 2 days) of the aggregate solution at room temperature (concentration: 10^{-3} mg mL^{-1}).

of the photoluminescence with the aging of the aggregate solution over 2 days suggested possible progressive changes in the morphology of the polymer aggregates.

The structures of the polymer aggregates formed in the $CHCl_3$–CH_3OH (v/v 1 : 9) solution were examined by transmission electron microscopy (TEM) and atomic force

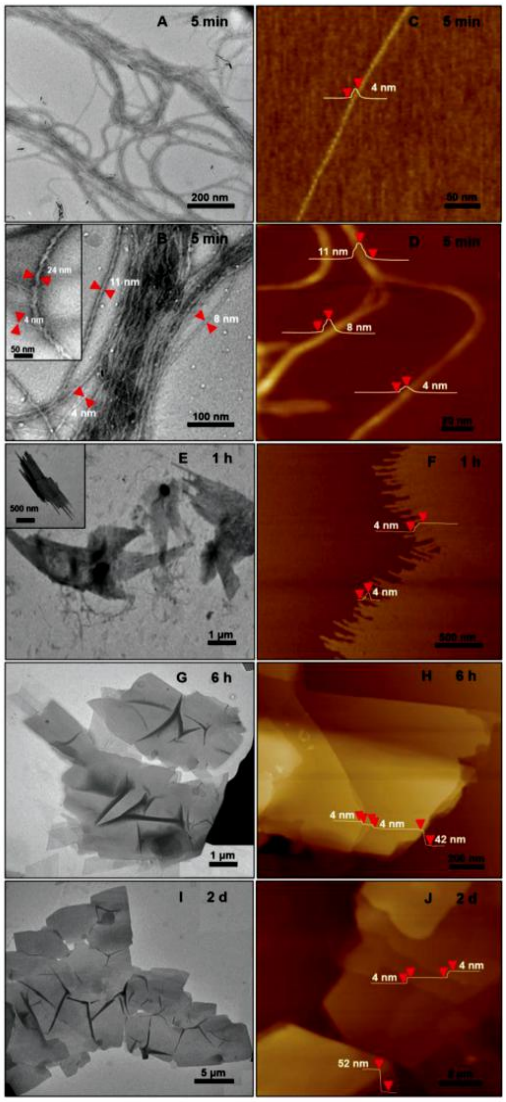

Fig. 3 TEM and AFM images of the assemblies formed by the hierarchical self-assembly of the graft copolymer in the $CHCl_3$–CH_3OH (v/v 1 : 9) solution after 5 minutes (A–D), 1 hours (E, F), 6 hours (G, H), 2 days (I, J). The relevant dimensions of the assemblies are indicated in the corresponding TEM and AFM images.

microscopy (AFM) (Fig. 3). TEM images revealed a 1D helical structure for the as-formed graft copolymer assemblies in $CHCl_3$–CH_3OH (Fig. 3A, B and Fig. S6A, B†). Left- and right-handed helices coexisted as no chiral moieties were employed during the self-assembly. The size statistics gave an average diameter of 17 ± 9 nm and lengths of 10–60 μm for the helices. The helices were formed by the twist of 1D aggregates of ~4 nm width (Fig. 3B and the inset shows a typical high-resolution TEM image). The AFM profiles gave a thickness of ~4 nm for the 1D aggregates and confirmed that they bundled into the helices (Fig. 3C and D). The combination of the 4 nm width and thickness manifests that the 1D aggregates are supermolecular nanowires. Since the thickness of the nanowires is close to the calculated width (~3.9 nm) of a graft copolymer molecule while their width is much smaller than the length (~36 nm) of the copolymer molecules (see the calculation in section 4.3.1 in page S12, ESI†), it is reasonable to speculate that the nanowires are assembled by an "end-to-end" and "side-by-side" combined alignment of the brush-like molecules, as illustrated in the middle of Fig. 1. The high-magnification TEM images (*e.g.* Fig. 3B) revealed that most of the helices (*ca.* 80%) were double- and triple-stranded in terms of their diameters and they coexisted with a number of multi-stranded helices (≥4 strands).

The formation of the helices was found to be kinetically controlled and they were thermodynamically unstable, namely their morphology was quenched temporarily in the mixed solvent with a large amount of CH_3OH and also in pure methanol after the dialysis of the $CHCl_3$–CH_3OH solution. After one-hour aging, the helices evolved into "rafts" that consisted of 1D nanostructures (Fig. 3E and F). The thickness of the rafts was ~4 nm (Fig. 3F), the same as that of the aforementioned nanowires. Therefore, it is believed that the rafts were single-layered and formed by the planar alignment of the nanowires. The unexpected transformation of 1D helical to 2D raft-like superstructures has never been documented before in 2D supramolecular self-assembly. With the aging of the aggregate solution for ~2 days, the rafts further developed into ultra-large sheets with an average thickness of 56 ± 4 nm and lateral dimensions of *ca.* 10 μm × 10 μm to 100 μm × 100 μm (Fig. 3G–J and S6D and E†). The greater thickness than that of the single-layered rafts indicated a multilayered structure of the sheets. The wrinkles observed by TEM on the nanosheets reflected a flexible feature (Fig. 3G, I and S6D†). Afterwards, no big changes were observed on the dimensions of the sheets. The ultra-large sheets suspended in solution were also observed by optical microscopy (Fig. S7†), confirming that the sheets were formed and free-standing in solution. Dynamic light scattering (DLS) measurements revealed an increase in the hydrodynamic diameter of the graft copolymer assemblies with the aging of their solution (Fig. 4 and S8†), confirming the progressive growth of the copolymer assemblies in $CHCl_3$–CH_3OH.

In light of previous studies on PEO crystallization-driven 2D self-assembly of polymers in solution,[24–26] we consider that PEO crystallization in organic media contributed to the solution-growth of the ultra-large multilayered sheets. Micro differential scanning calorimetry (μDSC) analysis gave a crystallization temperature (T_c) of ~26 °C for the PEO coils in the copolymer aggregates in $CHCl_3$–CH_3OH (Fig. S9†). Note that the 2D self-assembly of the graft copolymer occurred (at ~20 °C) below the T_c of the PEO chains. In addition, a short average distance of ~0.7 nm between neighboring PEO chains on the polyphenylene backbone would be favorable for the crystallization of the PEO coils if the graft copolymer aggregated into sheet-like structures, as the short distance resulted in a high number density of PEO chains at the sheet surfaces,

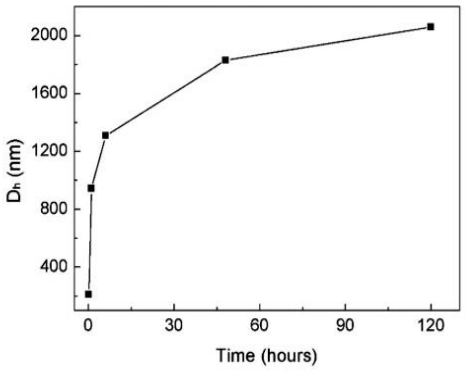

Fig. 4 DLS results showing an increase in the hydrodynamic diameter (D_h) of the graft copolymer assemblies with the aging of their solution at room temperature. The corresponding DLS plots are presented in Fig. S8.†

which exceeded the onset density for the crystallization of the PEO chains below their T_c (see the calculations in section 4.3.2 in the ESI, pages S13 and S14†).[26,27] Thus, it is reasonable to believe that the crystallization of the PEO chains acted as a key driving force for the formation of the ultra-large sheets. Two additional lines of evidence also support this point. First, the graft copolymer with a lower GP of ~60% did not form multilayered sheets under similar experimental conditions, probably due to the larger average distance between adjacent PEO coils on the polyphenylene backbone. Second, at a temperature (~30 °C) higher than the T_c of the PEO chains, the graft copolymer produced irregular aggregates rather than sheets in $CHCl_3$–CH_3OH.

Based on the above-mentioned results, a possible mechanism for the 1D to 2D hierarchical self-assembly of the graft copolymer is illustrated in Fig. 1. In the $CHCl_3$–CH_3OH solution, driven by the methanolphobic interaction, the graft copolymer first self-organized into 4 nm thin nanowires with a polyphenylene layer sandwiched by PEO coils on both up and down sides (middle of Fig. 1). Because of the relatively low PEO number density on the other two sides of the polyphenylene layer, the nanowires tend to associate to minimize the polyphenylene–methanol contact. Around the associated nanowires the PEO coils were crowded, as the estimated radius of gyration (R_g = ~1.5 nm (ref. 28)) of a 1 kg mol^{-1} PEO chain at its end-free state in solution is much larger than the short average distance of 0.7 nm between neighboring PEO chains in the graft copolymer in the nanowires. Hence, the steric interaction among the PEO chains drove the twist of the associated nanowires to provide more peripheral space for the PEO coils, thus leading to the formation of 1D helices. At this point, it is worth mentioning that although helix formation represents a self-assembly motif for some chiral polymers, owing to the ordered helical arrangement of their chiral moieties,[10,11,15] it rarely happens to achiral polymers;[9,29,30] nevertheless, in the present work, long helices were frequently found in the self-organization of the achiral graft copolymers in the $CHCl_3$–CH_3OH cosolvent system, which can be attributed to their unique rod–coil brush-like structure with a short average distance between adjacent PEO chains on the rigid polyphenylene backbone. However, since the helix formation occurred below the T_c of the PEO coils, the crystallization and the resulting compact state of the PEO chains alleviated their steric repulsion and thus favored the transformation of the helices to the thermodynamically more stable sheet-like structures. During the transformation, an untwist process of the helices could be considered for their transition to the single-layered rafts which further grew to the ultra-large multilayered sheets driven by the PEO crystallization.

Soft nanosheets with lateral dimensions of over 10 μm × 10 μm are quite difficult to achieve by the self-assembly of polymers in solution without support from a planar interface; only a few successful cases were documented.[21,22] In the present work, the rod–coil brush-like structure of the graft copolymer accounts for the ultra-large lateral sizes of the sheets, since the molecules of such an architecture incline to form assemblies with a sandwich structure, in which the laterally expanded poly-*para*-phenylene rigid backbones locate in the middle layer (Fig. 1). Such a sandwich structure along with the PEO crystallization is in favor of the growth of assemblies in 2D directions. Moreover, the rigid polyphenylene layer and the PEO crystallization can limit the rolling or closing of the sheets, which would generate tubes or vesicles as usually seen in the self-assembly of many flexible polymer systems.[23,31,32]

In summary, this work demonstrates a unique sheet formation by 1D to 2D hierarchical self-assembly of a rod–coil graft copolymer comprising a poly-*para*-phenylene backbone and PEO side chains. Driven by the methanolphobic interaction of the polyphenylene and the crystallization of the PEO chains in a $CHCl_3$–CH_3OH mixed organic solvent, the graft copolymer exhibited an unprecedented hierarchical self-assembly process from nanowires to 10–60 μm ultralong helices, then to single-layered "rafts", and finally to ultra-large multilayered nanosheets with lateral dimensions of *ca.* 10 μm × 10 μm to 100 μm × 100 μm. The rod–coil graft polymers afford a new chance for the so far challenging preparation of ultra-large self-assembled nanosheets in solution, as well as a novel system for fundamental studies on 2D self-assembly of conjugated polymers, including the mechanism, factors affecting the morphology, potential applications, *etc*.

Acknowledgements

The authors acknowledge the financial support from the 973 Programs of China (2012CB933404 and 2013CBA01602), the Natural Science Foundation of China (21320102006, 21304057 and 51573091), the Natural Science Foundation of Shanghai (13ZR1421200), the Program for Eastern Scholar in Shanghai, and the MPI Partner Group Project for Polymer Chemistry of Graphene Nanoribbons. The authors also appreciate the Instrumental Analysis Center of Shanghai Jiao Tong University for some measurements.

Notes and references

1 J. Yuan, Y. Xu and A. H. E. Müller, *Chem. Soc. Rev.*, 2011, **40**, 640.
2 J. Rzayev, *ACS Macro Lett.*, 2012, **1**, 1146.
3 R. Verduzco, X. Li, S. L. Pesek and G. E. Stein, *Chem. Soc. Rev.*, 2015, **44**, 2405.
4 S. S. Sheiko, B. S. Sumerlin and K. Matyjaszewski, *Prog. Polym. Sci.*, 2008, **33**, 759.
5 C. Li, M. Liu, N. G. Pschirer, M. Baumgarten and K. Müllen, *Chem. Rev.*, 2010, **110**, 6817.
6 Y. Huang, Y. Mai, X. Yang, U. Beser, J. Liu, F. Zhang, D. Yan, K. Müllen and X. Feng, *J. Am. Chem. Soc.*, 2015, **137**, 11602.
7 S. A. Jenekhe and X. L. Chen, *Science*, 1998, **279**, 1903.
8 S. K. Patra, R. Ahmed, G. R. Whittell, D. J. Lunn, E. L. Dunphy, M. A. Winnik and I. Manners, *J. Am. Chem. Soc.*, 2011, **133**, 8842.
9 E. Lee, B. Hammer, J.-K. Kim, Z. Page, T. Emrick and R. C. Hayward, *J. Am. Chem. Soc.*, 2011, **133**, 10390.
10 R.-M. Ho, Y.-W. Chiang, S.-C. Lin and C.-K. Chen, *Prog. Polym. Sci.*, 2011, **36**, 376.
11 C. Cai, Y. Li, J. Lin, L. Wang, S. Lin, X.-S. Wang and T. Jiang, *Angew. Chem., Int. Ed.*, 2013, **52**, 7732.
12 Y. Zheng, H. Zhou, D. Liu, G. Floudas, M. Wagner, K. Koynov, M. Mezger, H.-J. Butt and T. Ikeda, *Angew. Chem., Int. Ed.*, 2013, **52**, 4845.
13 A. Yassar, L. Miozzo, R. Gironda and G. Horowitz, *Prog. Polym. Sci.*, 2013, **38**, 791.
14 A. C. Kamps, M. H. M. Cativo, M. Fryd and S.-J. Park, *Macromolecules*, 2014, **47**, 161.
15 J. F. Reuther, D. A. Siriwardane, R. Campos and B. M. Nova, *Macromolecules*, 2015, **48**, 6890.
16 H.-C. Ho, Y.-H. Lee, C.-A. Dai, R. A. Segalman and W.-F. Su, *Macromolecules*, 2009, **42**, 4208; S.-H. Lin, S.-J. Wu, C.-C. Ho and W.-F. Su, *Macromolecules*, 2013, **46**, 2725; C.-C. Ho, S.-J. Wu, S.-H. Lin, S. B. Darling and W.-F. Su, *Macromol. Rapid Commun.*, 2015, **36**, 1329.
17 J. H. Yao, K. Y. Mya, L. Shen, B. He, L. Li, Z. Li, Z. Chen, X. Li and K. P. Loh, *Macromolecules*, 2008, **41**, 1438.
18 C. Cai, J. Lin, T. Chen and X. Tian, *Langmuir*, 2010, **26**, 2791.
19 G. M. Miyake, R. A. Weitekamp, V. A. Piunova and R. H. Grubbs, *J. Am. Chem. Soc.*, 2012, **134**, 14249.
20 Y. Li, T. Jiang, S. Lin, J. Lin, C. Cai and X. Zhu, *Sci. Rep.*, 2015, **5**, 10137.
21 J.-K. Kim, E. Y. Lee, H. Jeong, J.-K. Lee, W.-C. Zin and M. Lee, *J. Am. Chem. Soc.*, 2007, **129**, 6082.
22 K. T. Nam, S. A. Shelby, P. H. Choi, A. B. Marciel, R. Chen, L. Tan, T. K. Chu, R. A. Mesch, B.-C. Lee, M. D. Connolly, C. Kisielowski and R. N. Zuckermann, *Nat. Mater.*, 2010, **9**, 454.
23 Y. Mai and A. Eisenberg, *Chem. Soc. Rev.*, 2012, **41**, 5969.
24 G. Rizis, T. G. M. van de Ven and A. Eisenberg, *Angew. Chem., Int. Ed.*, 2014, **53**, 9000.
25 J. R. Sun, X. S. Chen, C. L. He and X. B. Jing, *Macromolecules*, 2006, **39**, 3717.
26 R. M. Van Horn, J. X. Zheng, H.-J. Sun, M.-S. Hsiao, W.-B. Zhang, X.-H. Dong, J. Xu, E. L. Thomas, B. Lotz and S. Z. D. Cheng, *Macromolecules*, 2010, **43**, 6113.
27 J. X. Zheng, H. Xiong, W. Y. Chen, K. Lee, R. M. Van Horn, R. P. Quirk, B. Lotz, E. L. Thomas, A.-C. Shi and S. Z. D. Cheng, *Macromolecules*, 2006, **39**, 641.
28 The R_g for a PEO chain at its end-free state in solution is estimated using $R_g^2 = b^2N_b/6$ from: M. Rubenstein and R. H. Colby, *Polymer Physics*, Oxford University Press, New York, 2004, where b = 0.8 nm for PEO.
29 S. Zhang, H. Cui, Z. Chen, K. L. Wooley and D. J. Pochan, *Soft Matter*, 2008, **4**, 90.
30 J. Dupont, G. Liu, K.-I. Niihara, R. Kimoto and H. Jinnai, *Angew. Chem., Int. Ed.*, 2009, **48**, 6144.
31 Y. Zhou and D. Yan, *Chem. Commun.*, 2009, 1172.
32 A. Blanazs, S. P. Armes and A. J. Ryan, *Macromol. Rapid Commun.*, 2009, **30**, 267.

(19)中华人民共和国国家知识产权局

(12)发明专利申请

(10)申请公布号 CN 105551831 A
(43)申请公布日 2016.05.04

(21)申请号 201610015124.6

(22)申请日 2016.01.11

(71)申请人 上海交通大学
地址 200240 上海市闵行区东川路800号

(72)发明人

(74)专利代理机构 上海旭诚知识产权代理有限公司 31220
代理人

(51)Int.Cl.
H01G 11/86(2013.01)
H01G 11/32(2013.01)
H01G 11/24(2013.01)

权利要求书1页 说明书5页 附图3页

(54)发明名称

一种碗状氮掺杂碳中空粒子的制备方法及应用

(57)摘要

本发明公开了一种碗状氮掺杂碳中空粒子的制备方法，包括：通过两亲的PS-b-PEO嵌段共聚物在溶液中自组装，形成完全塌陷的碗状囊泡；以碗状囊泡为模板支撑多巴胺在PEO链段上聚合，得到碗状聚多巴胺@Kippah囊泡粒子；将碗状聚多巴胺@Kippah囊泡粒子在氮气流下经过两步煅烧，得到碗状氮掺杂碳中空粒子。本发明的制备方法简便可行、成功率和转化率高、能有效降低制备成本。本发明还公开了一种碗状氮掺杂碳中空粒子的应用。本发明首次将碗状氮掺杂碳中空粒子以电极材料应用于超级电容器，获得了极高的电容量、良好的容量保持率和突出的循环稳定性。

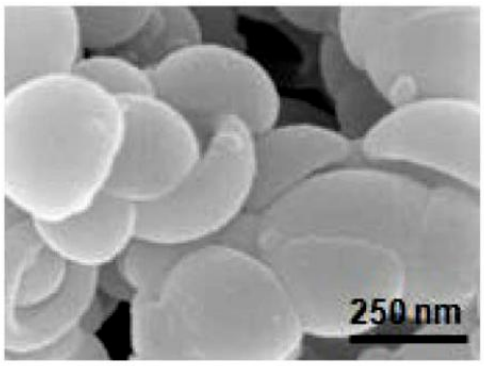

CN 105551831 A

1.一种碗状氮掺杂碳中空粒子的制备方法,其特征在于,包括以下步骤:

步骤一,向溶解了两亲的PS-b-PEO嵌段共聚物的二氧六环溶液中加入去离子水,所述PS-b-PEO嵌段共聚物在所述二氧六环溶液中自组装形成囊泡,当加入的去离子水量达到溶液总质量的50%时,迅速加入超过10倍于之前加入的去离子水的水量,使所述PS-b-PEO嵌段共聚物在所述二氧六环溶液中自组装形成的囊泡塌陷,得到碗状囊泡,即Kippah囊泡;其中所述溶液总质量指的是即PS-b-PEO嵌段共聚物+二氧六环溶液+去离子水的总质量;

步骤二,以步骤一得到的Kippah囊泡为模板支撑多巴胺在PEO链段上聚合,得到碗状聚多巴胺@Kippah囊泡粒子;

步骤三,将步骤二得到的碗状聚多巴胺@Kippah囊泡粒子在氮气流下经过两步煅烧,得到碗状氮掺杂碳中空粒子。

2.根据权利要求1所述的碗状氮掺杂碳中空粒子的制备方法,其特征在于,步骤一中,所述PS-b-PEO嵌段共聚物的质量为10～20mg,所述二氧六环溶液的体积为1-4mL。

3.根据权利要求2所述的碗状氮掺杂碳中空粒子的制备方法,其特征在于,所述二氧六环溶液的体积为1mL。

4.根据权利要求1所述的碗状氮掺杂碳中空粒子的制备方法,其特征在于,步骤一中的所述PS-b-PEO嵌段共聚物为PS_{370}-B-PEO_{114}。

5.根据权利要求1所述的碗状氮掺杂碳中空粒子的制备方法,其特征在于,步骤三中,两步煅烧包括第一煅烧和第二煅烧,且先进行第一煅烧再进行第二煅烧;其中,所述第一煅烧为300～500℃下煅烧3h,所述第二煅烧为800～1000℃下煅烧2h。

6.根据权利要求5所述的碗状氮掺杂碳中空粒子的制备方法,其特征在于,所述第一煅烧为400℃下煅烧3h,所述第二煅烧为900℃下煅烧2h。

7.根据权利要求1所述的碗状氮掺杂碳中空粒子的制备方法,其特征在于,步骤二中,取10-20mg多巴胺加入步骤一得到的含有Kippah囊泡的溶液中,得到的混合物在室温下温和地搅拌1～2h,然后加入20mg三羟甲基氨基甲烷盐酸盐,室温下搅拌反应48h使多巴胺聚合,聚合后得到的产物经过4-5次水洗离心,并经过冷冻干燥12～24h后得到碗状聚多巴胺@Kippah囊泡粒子。

8.根据权利要求7所述的碗状氮掺杂碳中空粒子的制备方法,其特征在于,步骤二中,取20mg多巴胺加入步骤一得到的含有Kippah囊泡的溶液中,得到的混合物在室温下温和地搅拌1h,然后加入20mg三羟甲基氨基甲烷盐酸盐,室温下搅拌反应48h使多巴胺聚合,聚合后得到的产物经过5次水洗离心,并经过冷冻干燥12h后得到碗状聚多巴胺@Kippah囊泡粒子。

9.根据权利要求1所述的碗状氮掺杂碳中空粒子的制备方法,其特征在于,步骤三中,将步骤二得到的碗状聚多巴胺@Kippah囊泡粒子转移到石英舟中,在管式炉中煅烧,并在氮气流下先400℃下煅烧3h,再900℃下煅烧2h,煅烧后自然冷却到室温,得到碗状氮掺杂碳中空粒子。

10.一种根据权利要求1-9中任意一项所述的碗状氮掺杂碳中空粒子作为电极材料在超级电容器中的应用。

一种碗状氮掺杂碳中空粒子的制备方法及应用

技术领域

[0001] 本发明涉及一种应用于超级电容器上的电极材料，尤其涉及一种碗状氮掺杂碳中空粒子的制备方法及应用。

背景技术

[0002] 近年来，超级电容器成为一种重要的能源存储设备，其性能受电极材料性质的极大制约。为开发高性能的电极材料，研究人员致力于制备新型碳材料，包括多孔碳、碳球、碳纤维、碳纳米管、石墨烯等。其中，中空结构碳球由于其多级孔结构大大有利于提高材料性能备受关注。但是，中空结构碳球的一个主要缺点是空腔引起的体积密度低，导致实际应用中低的体积容量。为了克服此缺点，许多研究都集中在制备复杂的中空结构，例如碗状中空材料上。碗状中空材料在保持中空结构优势的同时，可以减少多余的内腔容量，增加体积密度，从而使实际应用中的体积容量大大增加。

[0003] 例如，2014年Xiongwen Lou等人利用空心聚苯乙烯球作为模板制备了碗状中空结构的碳/SnO_2颗粒，在保持中空结构优势的同时，减少多余的内腔容量，使体积密度增加了30％。作为锂离子电池的负极材料，表现出优异的电化学性能(Angew.Chem.Int.Ed.2014,53,12803.)

[0004] 然而，现有的用空心聚苯乙烯球作为模板的制备方法包括中空聚苯乙烯球的合成、中空聚苯乙烯球水溶液的挥发以及干燥中空粒子在水中的再分散，其操作复杂且受环境因素影响大，成功率低。另外，用空心聚苯乙烯球作为模板，使得用水溶液挥发得到碗状中空结构的碗状产率较低，所得到的碗状中空粒子仅占很小一部分比例，所得产物的品质较低。同时，用空心聚苯乙烯球作为模板的制备方法耗时多，且因为产率低造成制备成本较高。

发明内容

[0005] 有鉴于现有技术的上述缺陷，本发明所要解决的技术问题是提供一种简便可行、成功率和转化率高、能降低成本的碗状中空粒子的制备方法，该方法制备的碗状中空粒子在保证电极材料良好的导电性的同时，还具有高体积能量密度，并具有优异的电容性能。

[0006] 为实现上述目的，本发明提供了一种碗状氮掺杂碳中空粒子的制备方法，包括以下步骤：

[0007] 步骤一，向溶解了两亲的PS-b-PEO嵌段共聚物的二氧六环溶液中加入去离子水，PS-b-PEO嵌段共聚物在二氧六环溶液中自组装形成囊泡，当加入的去离子水量达到溶液总质量(即PS-b-PEO嵌段共聚物+二氧六环溶液+去离子水的总质量)的50％时，迅速加入超过10倍于之前加入的去离子水的水量，使PS-b-PEO嵌段共聚物在二氧六环溶液中自组装形成的囊泡塌陷，得到碗状囊泡，即Kippah囊泡，这是一种具有圆顶状的完全塌陷的囊泡；Kippah囊泡的形成原理为，随着去离子水的加入，PS-b-PEO嵌段共聚物在二氧六环溶液中自组装形成囊泡，随着水量的迅速增加，囊泡内部二氧六环向外扩散，外部的去离子水向囊

泡内部扩散，由于二氧六环扩散速度高于水扩散速度，造成囊泡内形成负压，驱动囊泡凹陷，凹陷结构在过量的去离子水中被固定下来，即形成Kippah囊泡。

[0008] 步骤二，以步骤一得到的Kippah囊泡为模板支撑多巴胺在PEO链段上聚合，得到碗状聚多巴胺@Kippah囊泡粒子，即多巴胺包覆的碗状囊泡粒子；

[0009] 步骤三，将步骤二得到的碗状聚多巴胺@Kippah囊泡粒子在氮气流下经过两步煅烧，得到碗状氮掺杂碳中空粒子。

[0010] 优选地，步骤一中，PS-b-PEO嵌段共聚物的质量为10～20mg，二氧六环溶液的体积为1-4mL，进一步优选地，二氧六环溶液的体积为1mL。

[0011] 优选地，步骤一中PS-b-PEO嵌段共聚物为PS_{370}-B-PEO_{114}(其中下标数字表示PS-b-PEO嵌段聚合物的聚合度)。

[0012] 优选地，步骤三中，两步煅烧包括第一煅烧和第二煅烧，且先进行第一煅烧再进行第二煅烧；其中，第一煅烧为300～500℃下煅烧3h，第二煅烧为800～1000℃下煅烧2h。

[0013] 进一步优选地，第一煅烧为400℃下煅烧3h，第二煅烧为900℃下煅烧2h。

[0014] 优选地，步骤二中，取10-20mg多巴胺加入步骤一得到的含有Kippah囊泡的溶液中，得到的混合物在室温下温和地搅拌1～2h，然后加入20mg三羟甲基氨基甲烷盐酸盐，室温下搅拌反应48h使多巴胺聚合，聚合后得到的产物经过4-5次水洗离心，并经过冷冻干燥12～24h后得到碗状聚多巴胺@Kippah囊泡粒子。

[0015] 进一步优选地，步骤二中，取20mg多巴胺加入步骤一得到的含有Kippah囊泡的溶液中，得到的混合物在室温下温和地搅拌2h，然后加入20mg三羟甲基氨基甲烷盐酸盐，室温下搅拌反应24h使多巴胺聚合，聚合后得到的产物经过5次水洗离心，并经过冷冻干燥12h后得到碗状聚多巴胺@Kippah囊泡粒子。

[0016] 优选地，步骤三中，将步骤二得到的碗状聚多巴胺@Kippah囊泡粒子转移到石英舟中，在管式炉中煅烧，并在氮气流下先400℃下煅烧3h，再900℃下煅烧2h，煅烧后自然冷却到室温，得到碗状氮掺杂碳中空粒子。

[0017] 本发明还提供了一种碗状氮掺杂碳中空粒子作为电极材料在超级电容器中的应用。

[0018] 本发明的碗状氮掺杂碳中空粒子的制备方法简便可行、成功率和转化率高、能有效地降低制备成本。

[0019] 本发明在碗状碳中空结构的基础上结合氮掺杂的优势，获得了导电性能更优的高体积能量密度的碗状氮掺杂碳中空粒子，并且首次将其制作成电极材料应用于超级电容器，在0.1A/g的电流密度下，获得了365F/g得高电容量，在2.0A/g的电流密度下比容量也可以达到～200F/g，而且随着电流密度增加(直到10.0A/g)，该数值几乎不变，获得了高的容量保持率和循环稳定性。

[0020] 以下将结合附图对本发明的构思、具体结构及产生的技术效果作进一步说明，以充分地了解本发明的目的、特征和效果。

附图说明

[0021] 图1是本发明的实施例1的碗状氮掺杂碳中空粒子的制备原理图；

[0022] 图2是本发明的实施例1的碗状氮掺杂碳中空粒子的扫描电子显微镜图；

[0023] 图3是本发明的实施例1的碗状氮掺杂碳中空粒子的另一扫描电子显微镜图；

[0024] 图4是本发明的实施例1的碗状氮掺杂碳中空粒子的透射电子显微镜图；

[0025] 图5是本发明的实施例1的碗状氮掺杂碳中空粒子用于超级电容器所获得的电化学阻抗谱图；

[0026] 图6是本发明的实施例1的碗状氮掺杂碳中空粒子用于超级电容器所获得的体积电容曲线图。

具体实施方式

[0027] 实施例1：

[0028] 本发明的实施例1提供了一种碗状氮掺杂碳中空粒子的制备方法，包括以下步骤：

[0029] 步骤一，向溶解了10～20mg两亲的PS-b-PEO嵌段共聚物的1-4ml二氧六环溶液中加入去离子水(也可以为超纯水)，PS-b-PEO嵌段共聚物在二氧六环溶液中自组装形成囊泡，当加入的去离子水量达到溶液总质量(即PS-b-PEO嵌段共聚物+二氧六环溶液+去离子水的总质量)的50％时，迅速加入超过10倍于之前加入的去离子水的水量，使PS-b-PEO嵌段共聚物在二氧六环溶液中自组装形成的囊泡塌陷，得到碗状囊泡，即Kippah囊泡。

[0030] 步骤二，以步骤一得到的Kippah囊泡为模板支撑多巴胺在PEO链段上聚合，得到碗状聚多巴胺@Kippah囊泡粒子；具体地，取10～20mg多巴胺加入步骤一得到的含有Kippah囊泡的溶液中，得到的混合物在室温下温和地搅拌1～2h，然后加入20mg三羟甲基氨基甲烷盐酸盐，室温下搅拌反应48h使多巴胺聚合，聚合后得到的产物经过4～5次水洗离心，并经过冷冻干燥12～24h后得到碗状聚多巴胺@Kippah囊泡粒子，即多巴胺包覆的碗状囊泡粒子。

[0031] 步骤三，将步骤二得到的碗状聚多巴胺@Kippah粒子在氮气流下经过两步煅烧，得到碗状氮掺杂碳中空粒子；其中两步煅烧包括第一煅烧和第二煅烧，且先进行第一煅烧再进行第二煅烧；第一煅烧为300～500℃下煅烧3h，第二煅烧为800～1000℃下煅烧2h。

[0032] 图1为本实施例的碗状氮掺杂碳中空粒子的制备原理图。首先，向两亲的PS-b-PEO嵌段共聚物(以PS_{370}-B-PEO_{114}嵌段共聚物为例)的二氧六环溶液中加入去离子水得到囊泡。其中，疏水的PS段形成囊泡的壁，亲水的PEO形成囊泡表面的链段。再加入适当的水量后，二氧六环向囊泡外扩散和去离子水向囊泡内扩散所形成的压力差使囊泡向内凹陷成Kippah状。然后，用上述Kippah囊泡做模板，使多巴胺在PEO段上聚合，得到聚多巴胺@Kippah粒子。最后，将碗状的聚多巴胺@Kippah粒子煅烧裂解得到碗状氮掺杂碳中空粒子。

[0033] 图2为本实施例的碗状氮掺杂碳中空粒子的扫描电子显微镜图，其中显示了大范围碗状产物的形成，且形成的碗状氮掺杂碳中空粒子的直径D为450±55nm。图3和图4显示了碗状中空结构的形成，其中在单个的碗状氮掺杂碳中空粒子中，碗状氮掺杂碳中空粒子具有第一部和第二部，第一部和第二部构成封闭的中空的碗状，第一部或第二部的厚度T_s为23±1nm，第一部和第二部之间的距离T_c为35±2nm(参见图4)

[0034] 图5和图6分别为本实施例的碗状氮掺杂碳中空粒子应用于超级电容器的电化学阻抗谱图和比电容曲线图。图5显示碗状氮掺杂碳中空粒子用于超级电容器的阻抗约为1.3Ω，该阻抗值明显低于以往报道的氮掺杂碳中空粒子(约1.7Ω)，有利于提高超级电容器的额定输出功率。图6显示碗状氮掺杂碳中空粒子应用于超级电容器的体积容量在0.1A/g的电流密度下可高达365F/g。在2.0A/g的电流密度下体积容量也可以达到～200F/g，而且随

着电流密度增加(直到10.0A/g),该数值几乎不变。因而本实施例的碗状氮掺杂碳中空粒子应用于超级电容器表现出极高的体积电容、良好的容量保持率和突出的循环稳定性。

[0035] 实施例2:

[0036] 本发明的实施例2提供了一种碗状氮掺杂碳中空粒子的制备方法,包括以下步骤:

[0037] 步骤一,取10～20mg PS_{370}-B-PEO_{114}嵌段共聚物溶于1mL二氧六环溶液中,在室温下磁力搅拌1h后加入1mL加入超纯水,之后,快速加入20mL超纯水,得到碗状囊泡,即Kippah囊泡;

[0038] 步骤二,以步骤一得到的Kippah囊泡为模板支撑多巴胺在PEO链段上聚合,得到碗状聚多巴胺@Kippah粒子;具体地,取20mg多巴胺加入步骤一得到的含有Kippah囊泡的溶液中,得到的混合物在室温下温和地搅拌1h,然后加入20mg三羟甲基氨基甲烷盐酸盐室温下搅拌反应48h使多巴胺聚合,聚合后得到的产物经过5次水洗离心,并经过冷冻干燥12h后得到碗状聚多巴胺@Kippah粒子,即多巴胺包覆的碗状囊泡粒子。

[0039] 步骤三,将步骤二得到的碗状聚多巴胺@Kippah粒子转移到石英舟中,在管式炉中煅烧,并在氮气流下先400℃下煅烧3h,再900℃下煅烧2h,煅烧后自然冷却到室温,得到碗状氮掺杂碳中空粒子。

[0040] 实施例3:

[0041] 本发明的实施例3提供了一种碗状氮掺杂碳中空粒子的制备方法,包括以下步骤:

[0042] 步骤一,取10～20mg PS_{370}-B-PEO_{114}嵌段共聚物溶于4mL二氧六环溶液中,在室温下磁力搅拌1h后加入1mL超纯水,之后,快速加入20mL超纯水,得到碗状囊泡,即Kippah囊泡;

[0043] 步骤二,以步骤一得到的Kippah囊泡为模板支撑多巴胺在PEO链段上聚合,得到碗状聚多巴胺@Kippah粒子;具体地,取10mg多巴胺加入步骤一得到的含有Kippah囊泡的溶液中,得到的混合物在室温下温和地搅拌2h,然后加入20mg三羟甲基氨基甲烷盐酸盐室温下搅拌反应48h使多巴胺聚合,聚合后得到的产物经过4～5次水洗离心,并经过冷冻干燥24h后得到碗状聚多巴胺@Kippah粒子,即多巴胺包覆的碗状囊泡粒子。

[0044] 步骤三,将步骤二得到的碗状聚多巴胺@Kippah粒子转移到石英舟中,在管式炉中煅烧,并在氮气流下先300℃下煅烧3h,再800℃下煅烧2h,煅烧后自然冷却到室温,得到碗状氮掺杂碳中空粒子。

[0045] 实施例4:

[0046] 本发明的实施例4提供了一种碗状氮掺杂碳中空粒子的制备方法,包括以下步骤:

[0047] 步骤一,取10～20mg PS_{370}-B-PEO_{114}嵌段共聚物溶于3mL二氧六环溶液中,在室温下磁力搅拌1h后加入1mL超纯水,之后,快速加入20mL超纯水,得到碗状囊泡,即Kippah囊泡;

[0048] 步骤二,以步骤一得到的Kippah囊泡为模板支撑多巴胺在PEO链段上聚合,得到碗状聚多巴胺@Kippah粒子;具体地,取15mg多巴胺加入步骤一得到的含有Kippah囊泡的溶液中,得到的混合物在室温下温和地搅拌1～2h,然后加入20mg三羟甲基氨基甲烷盐酸盐室温下搅拌反应48h使多巴胺聚合,聚合后得到的产物经过4～5次水洗离心,并经过冷冻干燥18h后得到碗状聚多巴胺@Kippah粒子,即多巴胺包覆的碗状囊泡粒子。

[0049] 步骤三,将步骤二得到的碗状聚多巴胺@Kippah粒子转移到石英舟中,在管式炉中

煅烧，并在氮气流下先500℃下煅烧3h，再1000℃下煅烧2h，煅烧后自然冷却到室温，得到碗状氮掺杂碳中空粒子。

[0050] 以上详细描述了本发明的较佳具体实施例。应当理解，本领域的普通技术人员无需创造性劳动就可以根据本发明的构思作出诸多修改和变化。因此，凡本技术领域中技术人员依本发明的构思在现有技术的基础上通过逻辑分析、推理或者有限的实验可以得到的技术方案，皆应在由权利要求书所确定的保护范围内。

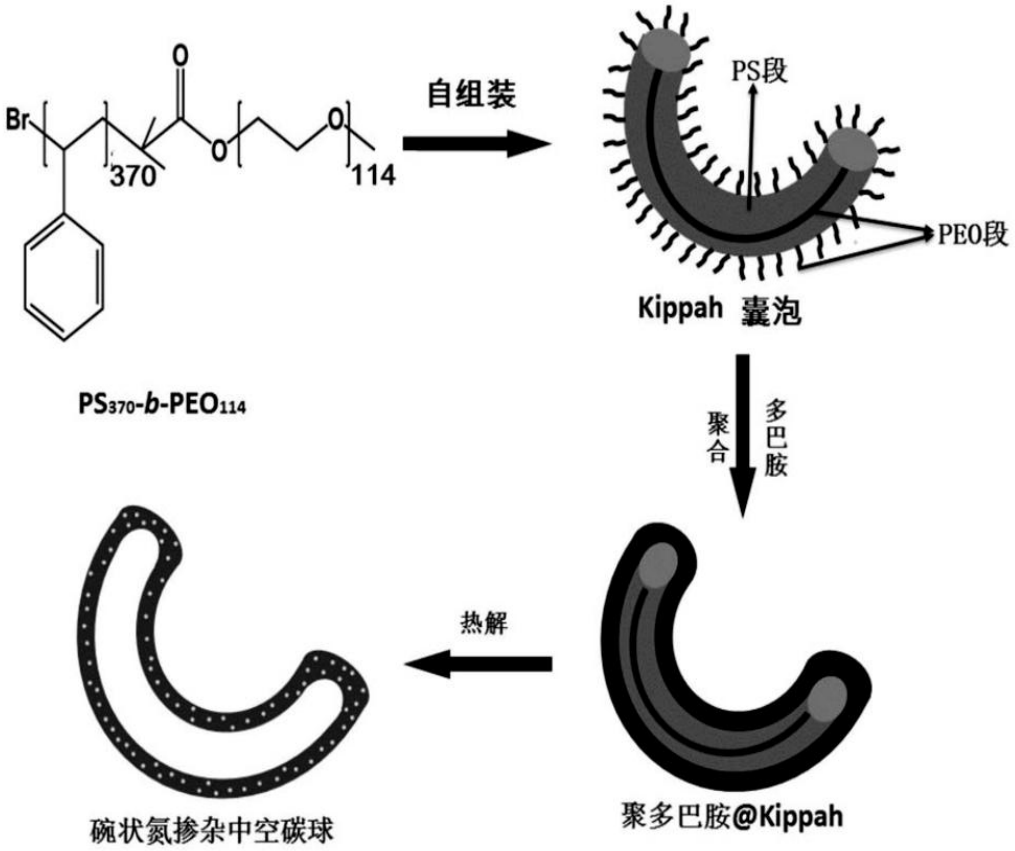
Br
O
O
O
370
114
自组装
PS段
PEO段
Kippah 囊泡
PS370-b-PEO114
聚合
多巴胺
热解
碗状氮掺杂中空碳球
聚多巴胺@Kippah

图1

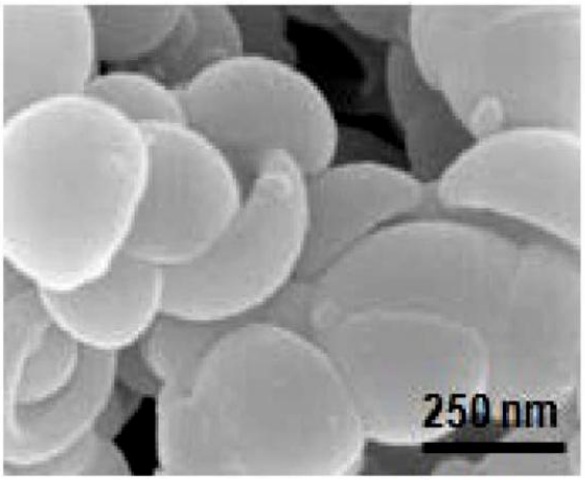
250 nm

图2

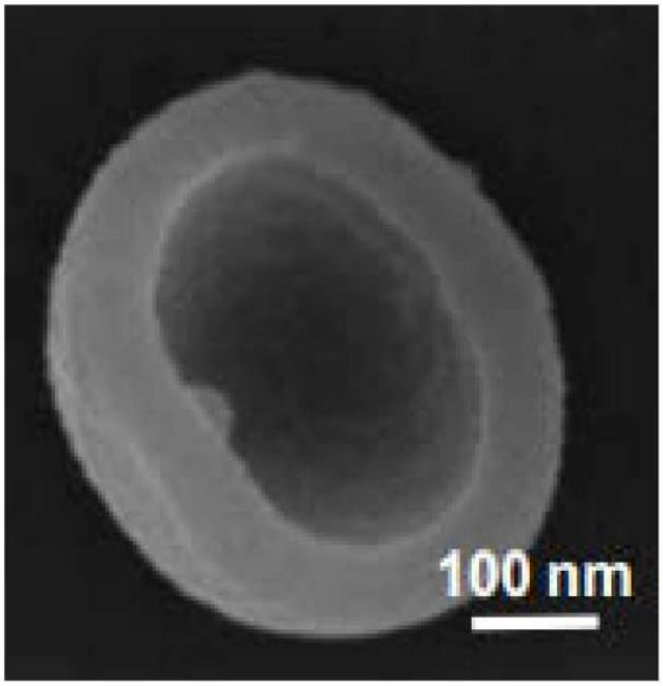

图3

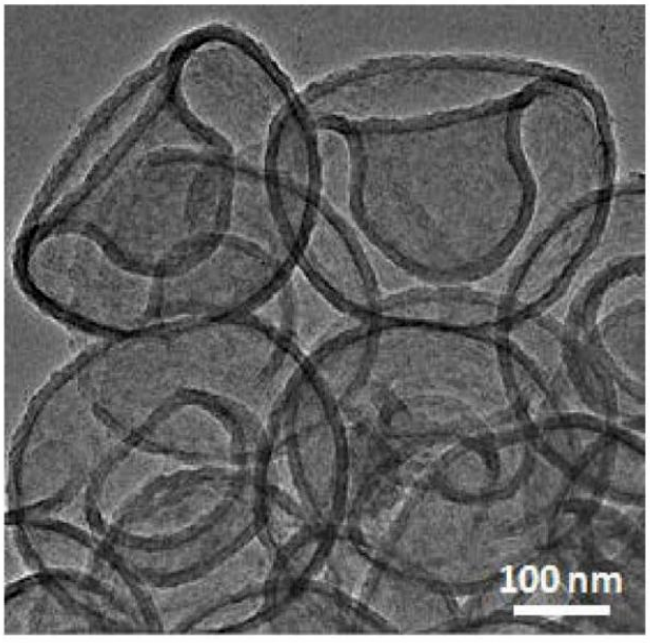

图4

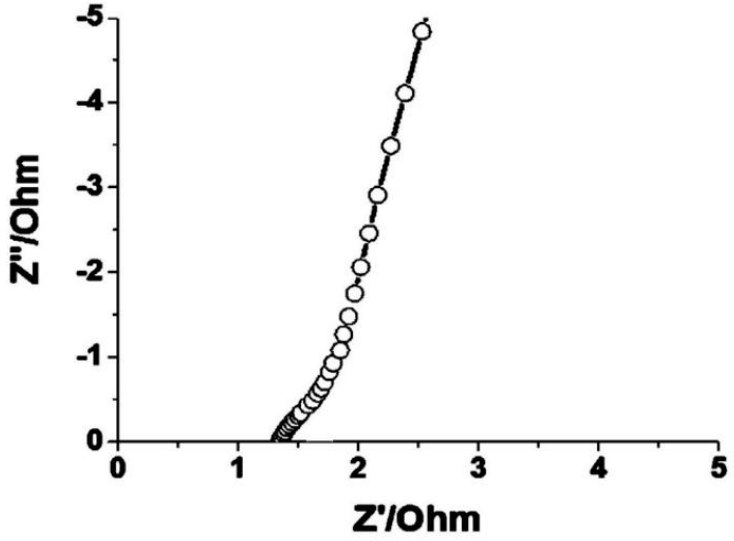
Z''/Ohm
Z'/Ohm
-5
-4
-3
-2
-1
0
0
1
2
3
4
5

图5

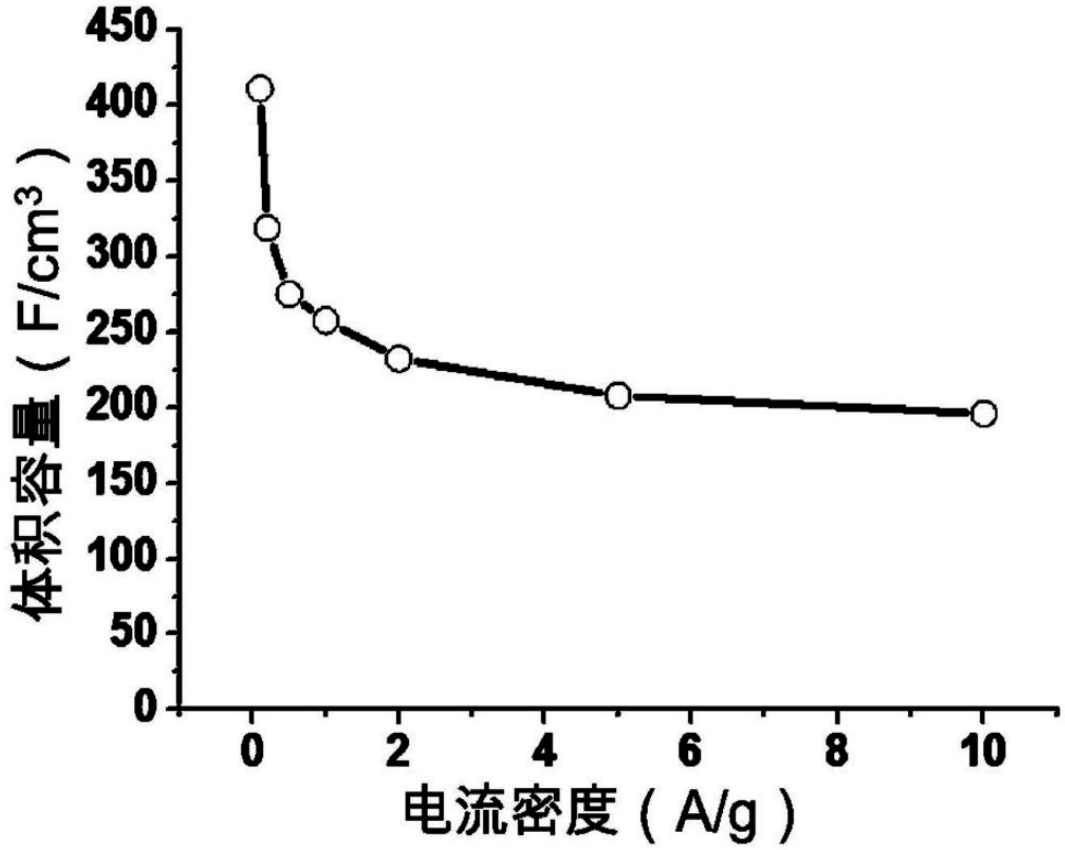
体积容量（F/cm³）
电流密度（A/g）
450
400
350
300
250
200
150
100
50
0
0
2
4
6
8
10

图6

(19)中华人民共和国国家知识产权局

(12)发明专利申请

(10)申请公布号 CN 105523540 A
(43)申请公布日 2016.04.27

(21)申请号 201610061161.0

(22)申请日 2016.01.28

(71)申请人 上海交通大学
地址 200240 上海市闵行区东川路800号

(72)发明人

(74)专利代理机构 上海旭诚知识产权代理有限公司 31220
代理人

(51)Int.Cl.
C01B 31/02(2006.01)

权利要求书2页 说明书5页 附图5页

(54)发明名称

一种孔径大小可控的介孔碳球材料的制备方法

(57)摘要

本发明公开了一种孔径大小可控的介孔碳球材料的制备方法，包括如下步骤：步骤1，聚环氧乙烷单甲醚溶解在甲苯中；步骤2，加入溴代化合物，沉淀，干燥萃取；步骤3，加入CuBr和联二吡啶（反应催化剂）；步骤4，苯乙烯除氧；步骤5，将步骤4中的纯净物加入到步骤3的混合物中；步骤6，搅拌，过柱，沉淀，真空干燥；步骤7，加入前驱体多巴胺，净化煅烧，得产物。本发明的制备方法具有如下优点：1、方法简单，常温下制备，设备易操作；2、所需试剂均低毒性或无毒性，是一种环保的制备方法；3、制备方法可制备孔径大，且能精确调节孔径大小的介孔球；4、N掺杂的介孔碳球可作为一种高性能储能材料，首次应用在超级电容器上。

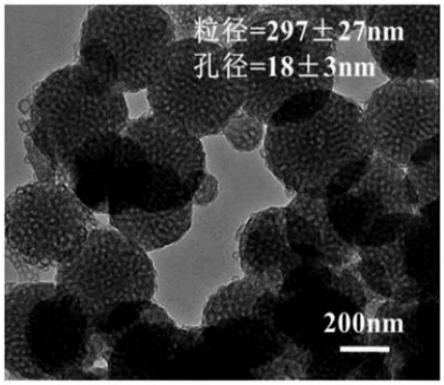

CN 105523540 A

1.一种孔径大小可控的介孔碳球材料的制备方法,其特征在于,包括如下步骤:

步骤1,聚环氧乙烷单甲醚溶解在甲苯中,共沸蒸馏除去来自所述聚环氧乙烷单甲醚中的水,冷却得到第一溶液;

步骤2,在所述第一溶液中加入溴代化合物,室温下搅拌反应过夜,旋转蒸发除去所述甲苯的80%-90%,再加入乙醚形成第一沉淀;所述第一沉淀先真空干燥再溶解在水中然后用二氯甲烷萃取,收集萃取得到的有机层,用$MgSO_4$干燥,而后真空旋转蒸发除去所述二氯甲烷,得到引发剂;

步骤3,先将所述引发剂加入到Schlenk瓶中,再将CuBr和联二吡啶加入到所述Schlenk瓶中,充分混合得到第一混合物,所述第一混合物在惰性气体保护下除去氧;

步骤4,苯乙烯先经中性氧化铝柱过滤除去阻聚剂,再利用鼓氮气法除去所述苯乙烯中的氧,得到苯乙烯纯净物;

步骤5,将所述苯乙烯纯净物加入到所述Schlenk瓶中与所述第一混合物混合得到第二混合物,所述第二混合物先在室温下搅拌10分钟,然后在恒温油浴下加热到100-120℃并不断搅拌反应5-12h,得到第三混合物;

步骤6,所述第三混合物加入四氢呋喃溶剂中得到第四混合物,所述第四混合物经中性氧化铝过柱,再加入过量甲醇并过滤得到第二沉淀,所述第二沉淀再用甲醇洗然后在40℃真空条件下干燥两天,得到嵌段聚合物;

步骤7,所述嵌段聚合物溶解在四氢呋喃中得到第二溶液,将乙醇和去离子按体积比1:2配成乙醇溶液,将所述乙醇溶液加入到所述第二溶液中,产生胶束聚集体;将盐酸多巴胺前驱体在搅拌条件下加入到所述第二溶液中,室温下搅拌48h以便多巴胺的聚合;收集产物离心净化,最后高温煅烧,得到所述介孔碳球。

2.根据权利要求1所述的一种孔径大小可控的介孔碳球材料的制备方法,其特征在于,步骤1中,所述聚环氧乙烷单甲醚的聚合度为100～500。

3.根据权利要求1所述的一种孔径大小可控的介孔碳球材料的制备方法,其特征在于,步骤1中,在0℃条件下,所述聚环氧乙烷单甲醚溶解在所述甲苯中。

4.根据权利要求1所述的一种孔径大小可控的介孔碳球材料的制备方法,其特征在于,步骤2中,所述溴代化合物是2-溴异丁酰溴。

5.根据权利要求4所述的一种孔径大小可控的介孔碳球材料的制备方法,其特征在于,所述2-溴异丁酰溴与所述聚环氧乙烷单甲醚的物质的量比为1:(0.1～1.0)。

6.根据权利要求1所述的一种孔径大小可控的介孔碳球材料的制备方法,其特征在于,步骤3中,所述CuBr预先用冰醋酸提纯。

7.根据权利要求1所述的一种孔径大小可控的介孔碳球材料的制备方法,其特征在于,步骤3中,所述CuBr和所述联二吡啶的质量比为1:(2.0～5.0)。

8.根据权利要求1所述的一种孔径大小可控的介孔碳球材料的制备方法,其特征在于,步骤3中,所述惰性气体包括氮气、氩气。

9.根据权利要求1所述的一种孔径大小可控的介孔碳球材料的制备方法,其特征在于,在步骤5中,改变所述苯乙烯的用量以精确调节所述介孔碳球的孔径。

10.根据权利要求1所述的一种孔径大小可控的介孔碳球材料的制备方法,其特征在于,步骤7中,所述高温煅烧是指:先在管式炉中氮气保护气氛下经350℃煅烧3h,然后每分

钟升温1℃，到达900℃后保温3h。

一种孔径大小可控的介孔碳球材料的制备方法

技术领域

[0001] 本发明涉及一种介孔材料的制备方法，具体涉及一种孔径大小可控的介孔碳球材料的制备方法，以及该介孔碳球材料在超级电容器方面的应用，属于纳米材料制备和电化学储能领域。

背景技术

[0002] 超级电容器是一种介于传统电容器和充电电池之间的新型储能装置，其容量可达几百至上千法拉。超级电容器储存电荷的能力比普通电容器高，并具有充放电速度快、效率高、对环境无污染、循环寿命长、使用温度范围宽、安全性高等特点。它可以作为便携式仪器设备、数据记忆存储系统的后备电源以及作为电动汽车的储能部件或内燃机车的启动电源。然而，超级电容器的能量密度比二次电池小，为了超级电容器能够应用到各种实际设备当中，具有高功率密度和能量密度的超级电容器是亟需开发的。

[0003] 介孔，特别是大尺寸的介孔，更容易实现反应大分子的介质传输。形貌控制是一个关键的因素。球形形貌，尤其是粒径小于200nm的球，越来越受到关注，因为球形提供了介质传递的短路径且降低了粘滞效应。大量文献报道了使用球状碳材料在药物输送，基因治疗，超级电容器，锂硫电池，二氧化碳捕获等方面的应用。从现有技术来看，许多方法能够制备介孔碳球，包括Stober法、硬模板和软模板方法。例如，Lu团队(Adv.Mater.2013,25,998)通过直接自聚合和随后的碳化合成120至800nm粒径的微孔碳球。虽然用KOH刻蚀后所得到的碳球具有高的比表面积，但得到的球形孔仍是微孔其孔径小于2nm。Zhao团队(Angew.Chem.Int.Ed.2010,49,7987;Angew.Chem.2010,122,8159)利用水热方法，以酚醛树脂和F127的共组装合成了有序的介孔碳球。然而，他们的孔径为3nm。这样的孔径显著降低了其实际应用。

[0004] 目前，通过用许多高分子量的嵌段聚合物(如PS-b-PEO、PIB-b-PEO、PS-b-P4VP和PEO-b-PMMA)做软模板制备了孔径大于10nm的介孔材料。但是，它们大都形成了薄膜或形状不规则的微米颗粒。这些体系涉及溶剂蒸发过程不适用于制备介孔碳球。大尺寸的孔的介孔碳球的应用会更广泛。

[0005] 掺杂有杂原子的碳纳米材料，如氮、硼和硫，由于电子给体/受体的特性和所得到的电化学性能的增强吸引了许多的关注。氮掺杂的碳纳米材料，如氮掺杂碳纳米管，石墨烯和介孔碳，都表现出优异的电性能和良好的氧还原稳定性。因此，大孔径尺寸氮掺杂的介孔碳球肯定会通过减少扩散路径增强介质传递。若介孔碳球材料孔径太小，由于电解质离子难以进入其中，使得这些微孔所对应的比表面积对电容没有贡献。在充放电的过程当中，电解液不能够充分接触，尤其是有机电解液，其包含大的有机分子，在高负荷的电流密度下，微孔内裸露的表面不能够充分进行电量存储。大尺寸的介孔，大分子的介质传递更容易实现，能够增强超级电容器的性能。然而，目前介孔球的孔径太小，限制了实际的应用。

[0006] 现有技术制备介孔碳球材料存在以下技术问题：

[0007] 1、利用硬模板制备的介孔碳球步骤繁琐，程序复杂，有毒污染性强。

[0008] 2、目前制备方法反应条件苛刻。

[0009] 3、现有技术制备的介孔球的孔径太小，应用受限。

发明内容

[0010] 本发明针对现有技术的上述不足，首次提供一种孔径大小可控的介孔碳球材料的制备方法，可制备孔径大，且能精确调节孔径大小的介孔球。首先，通过ATRP(原子转移自由基聚合)方法制备PS-b-PEO(聚苯乙烯嵌段聚环氧乙烷)嵌段聚合物，然后利用多巴胺(DA)与胶束协同组装并自聚后经高温焙烧，实现了温和温度下N掺杂的介孔碳球的制备。作为一种高性能储能材料，应用在超级电容器上。

[0011] 本发明的原理是：利用原子转移自由基聚合合成一系列具有不同憎水链长度的PS-b-PEO，并利用嵌段聚合物自组装原理，将这些聚合物组装成具有不同粒径的PS-b-PEO胶束。在常温条件下，利用多巴胺前驱体的自聚反应，包裹粒径不一的胶束，获得由PS-b-PEO/聚多巴胺复合微球，后经高温焙烧得到具有不同孔径的氮掺杂介孔碳。

[0012] 本发明的第一方面，提供了一种孔径大小可控的介孔碳球材料的制备方法，包括如下步骤：

[0013] 步骤1，聚环氧乙烷单甲醚溶解在甲苯中

[0014] 聚环氧乙烷单甲醚溶解在甲苯中，共沸蒸馏除去来自聚环氧乙烷单甲醚中的水，冷却得到第一溶液；聚环氧乙烷单甲醚为白色粉末状。

[0015] 步骤2，加入溴代化合物，沉淀，干燥萃取

[0016] 在第一溶液中加入溴代化合物，室温下搅拌反应过夜，旋转蒸发除去甲苯的80%-90%，再加入乙醚形成第一沉淀；第一沉淀先真空干燥再溶解在水中然后用二氯甲烷萃取，收集萃取得到的有机层，用$MgSO_4$干燥，而后真空旋转蒸发除去二氯甲烷，得到引发剂。引发剂记作PEO-Br。

[0017] 步骤3，加入CuBr和联二吡啶

[0018] 先将引发剂加入到Schlenk瓶中，再将CuBr和联二吡啶加入到Schlenk瓶中，充分混合得到第一混合物，第一混合物在惰性气体保护下除去氧。

[0019] 步骤4，苯乙烯除氧

[0020] 苯乙烯先经中性氧化铝柱过滤除去阻聚剂，再利用鼓氮气法除去苯乙烯中的氧，得到苯乙烯纯净物。

[0021] 步骤5，将步骤4中的苯乙烯纯净物加入到步骤3的混合物中

[0022] 将苯乙烯纯净物加入到Schlenk瓶中与第一混合物混合得到第二混合物，第二混合物先在室温下搅拌10分钟，然后在恒温油浴下加热到100-120℃并不断搅拌反应5-12h，得到第三混合物。

[0023] 步骤6，搅拌，过柱，沉淀，真空干燥

[0024] 第三混合物加入四氢呋喃溶剂中得到第四混合物，第四混合物经中性氧化铝过柱，再加入过量甲醇并过滤得到第二沉淀，第二沉淀再用甲醇洗然后在40℃真空条件下干燥两天，得到嵌段聚合物。第四混合物中大部分为PS-b-PEO嵌段聚合物，其中可能含有少量PEO-Br，使用过量甲醇可洗去上述PEO-Br，得到纯净的PS-b-PEO嵌段聚合物。

[0025] 步骤7，加入前驱体多巴胺，净化煅烧，得产物

[0026] 嵌段聚合物溶解在四氢呋喃中得到第二溶液，将乙醇和去离子按体积比1:2配成乙醇溶液，将乙醇溶液加入到第二溶液中，产生胶束聚集体；将盐酸多巴胺前驱体在搅拌条件下加入到第二溶液中，室温下搅拌48h以便多巴胺的聚合；收集产物离心净化，最后高温煅烧，得到介孔碳球。介孔碳球可表示为PDA/PS-b-PEO。

[0027] 多巴胺前驱体可以用酚醛树脂代替。

[0028] 优选地，步骤1中，聚环氧乙烷单甲醚的聚合度为100～500。

[0029] 优选地，步骤1中，在0℃条件下，聚环氧乙烷单甲醚溶解在甲苯中。

[0030] 优选地，步骤2中，溴代化合物是2-溴异丁酰溴。更优选地，2-溴异丁酰溴与聚环氧乙烷单甲醚的物质的量比为1:(0.1～1.0)。

[0031] 优选地，步骤3中，CuBr预先用冰醋酸提纯。

[0032] 优选地，步骤3中，CuBr和联二吡啶的质量比为1:(2.0～5.0)。

[0033] 优选地，步骤3中，惰性气体包括氮气、氩气。

[0034] 优选地，在步骤5中，改变苯乙烯的用量以精确调节介孔碳球的孔径。

[0035] 优选地，步骤7中，高温煅烧是指：先在管式炉中氮气保护气氛下经350℃煅烧3h，然后每分钟升温1℃，到达900℃后保温3h。

[0036] 本发明的另一方面，还提供了一种孔径大小可控的介孔球材料的应用。

[0037] 本发明的介孔球材料首次应用在三电极的超级电容器体系中，在本发明的具体实施例中，介孔碳球作为超级电容器的电极材料，介孔碳球的电化学性能是在上海辰华仪器有限公司生产的电化学工作站中进行评估。三电极系统用1mol/L的H_2SO_4电解质进行恒电流充放电测量。工作电极通过混合质量分数80％的粉末状活性材料，质量分数10％的炭黑和质量分数10％聚四氟乙烯粘合剂制备。铂被用作对电极，Ag/AgCl电极用作参比电极。室温下在不同的电流密度中测试，其电位范围为0～1V(相对于Ag/AgCl电极)。

[0038] 本发明的有益效果是：

[0039] 1、方法简单，常温下制备，设备易操作；

[0040] 2、所需试剂均低毒性或无毒性，是一种环保的制备方法；

[0041] 3、制备方法可制备孔径大，且能精确调节孔径大小的介孔球；

[0042] 4、N掺杂的介孔碳球可作为一种高性能储能材料，首次应用在超级电容器上。

附图说明

[0043] 图1为按实施例1制备的PS-b-PEO胶束透射电镜图；

[0044] 图2为按实施例2制备的焙烧后PDA/PS-b-PEO透射电镜图；

[0045] 图3为按实施例2制备的焙烧后PDA/PS-b-PEO扫描电镜图；

[0046] 图4为按实施例3制备的N掺杂介孔碳球的氮气吸脱附曲线；

[0047] 图5为按实施例3制备的N掺杂介孔碳球的孔径分布曲线；

[0048] 图6为按实施例2制备的N掺杂介孔碳球的氮元素X射线能谱图；

[0049] 图7为按实施例4制备的N掺杂介孔碳球的电容量图；

[0050] 图8为按实施例5制备的N掺杂介孔碳球的充放电曲线；

[0051] 图9为按实施例5制备的N掺杂介孔碳球的循环稳定性曲线。

具体实施方式

[0052] 下面对本发明的实施例做详细说明，以下实施例在以本发明技术方案为前提下进行实施，给出了详细的实施方式和具体的操作过程，但本发明的保护范围不限于下述的实施例。

[0053] 实施例1

[0054] 在一个500mL的三口烧瓶中，25.0g的PEO114-OH(114是聚环氧乙烷单甲醚的聚合度)溶解在100mL的甲苯中。低压共沸蒸馏除去水，溶液冷却到0℃。2.47mL 2-溴异丁酰溴通过注射器逐滴加入，室温下搅拌反应过夜。加入十倍过量的乙醚形成沉淀。得到的原料真空干燥，然后用二氯甲烷萃取。收集有机层，真空下移去溶剂，形成纯净的大分子引发剂。0.067g CuBr和0.22g联二吡啶加入到Schlenk瓶中，Schlenk瓶抽真空，补氮气，如此循环几次除去氧气。然后将8mL苯乙烯转移到大分子引发剂Schlenk瓶中，得到的深棕色的混合物在室温下搅拌10分钟。恒温油浴下加热到120℃反应8h。加入大量的THF溶剂，过柱，加入过量甲醇沉淀，过滤沉淀然后用甲醇洗，最终的产品40℃真空干燥两天。嵌段聚合物溶解在2mL四氢呋喃中，然后，6mL的乙醇和去离子水混合液(体积比1:2)缓慢加入到上述溶液中，产生了胶束聚集体。从图1中可以看出，球形胶束分散均匀，尺寸均一，粒径约20nm。

[0055] 实施例2

[0056] 在一个500mL的三口烧瓶中，25.0g的PEO114-OH溶解在100mL的甲苯中。低压共沸蒸馏除去水，溶液冷却到0℃。2.47mL 2-溴代异丁酰溴通过注射器逐滴加入，室温下搅拌反应过夜。乙醚沉淀，原料干燥，二氯甲烷萃取。真空下移去溶剂。0.067g CuBr和0.22g联二吡啶加入到Schlenk瓶中，然后除氧的8mL苯乙烯转移到大分子引发剂Schlenk瓶中，得到的深棕色的混合物在室温下搅拌10分钟。恒温油浴下加热到120℃反应8h。后处理得到的嵌段聚合物溶解在2mL四氢呋喃中，然后，6mL的乙醇和去离子水混合液(体积比1:2)缓慢加入到上述溶液中。然后，0.124g的盐酸多巴胺在中速搅拌下加入到溶液中。1h后，0.3mL的NH_4OH(28wt%)注入到混合物中，室温下搅拌48h以便多巴胺的聚合。收集产物，离心净化，然后用乙醇和去离子水洗去，最后，收集的产物在40℃干燥两天。产生的PDA/PS165-b-PEO114球(165是聚苯乙烯的聚合度)在管式炉中N_2保护350℃下烧3h，最后每分钟升温1℃到达900℃，再保温3h。

[0057] 从图2和图3中可以看出，热处理以后，电镜图明显呈现介孔球形结构。即胶束模板脱除后，介孔球纳米粒子里面出现球形孔。PS-b-PEO在碳化过程中作为成孔剂，形成介孔碳球。

[0058] 从图6中可以看出，介孔碳球中掺杂有氮元素，吡啶型氮和石墨型氮均有，并且主要为石墨型氮。

[0059] 实施例3

[0060] 实施内容是在实施例2的基础上，改变苯乙烯的用量，分别为3mL、8mL、15mL、20mL、22.5mL，其它条件不变。

[0061] 从图4中可以看出，曲线均有回滞环，说明均为介孔材料。

[0062] 从图5中可以看出，孔径从20-40nm均有分布，随着PS链长的增加，孔径也增加。

[0063] 实施例4

[0064] 以实施例3所得的电极材料，在三电极系统中用1mol/L的H_2SO_4做电解质。工作电极是质量分数80％的粉末状活性材料，质量分数10％的炭黑和质量分数10％聚四氟乙烯粘合剂的混合，铂被用作负电极，Ag/AgCl电极用作参比电极。

[0065] 从图7中可以看出，MCNS-62的性能最好。N掺杂的介孔碳球具有高容量的双层电容行为。

[0066] 实施例5

[0067] 实施内容前半部分基本同实施例2，所不同的是苯乙烯的添加量改为3mL，得到PDA/PS62-b-PEO114碳球。在三电极系统中用1mol/L的H_2SO_4做电解质。工作电极是质量分数80％的粉末状活性材料，质量分数10％的炭黑和质量分数10％聚四氟乙烯粘合剂的混合，铂被用作负电极，Ag/AgCl电极用作参比电极。

[0068] 从图8中可以看出，恒电流充放电测试呈现三角曲线，证明是有效的离子传输。

[0069] 从图9中可以看出，循环稳定性曲线中，10A/g的电流密度下，10000次充放循环仍能稳定。具有极好的循环稳定性。

[0070] 以上详细描述了本发明的较佳具体实施例。应当理解，本领域的普通技术人员无需创造性劳动就可以根据本发明的构思作出诸多修改和变化。因此，凡本技术领域中技术人员依本发明的构思在现有技术的基础上通过逻辑分析、推理或者有限的实验可以得到的技术方案，皆应在由权利要求书所确定的保护范围内。

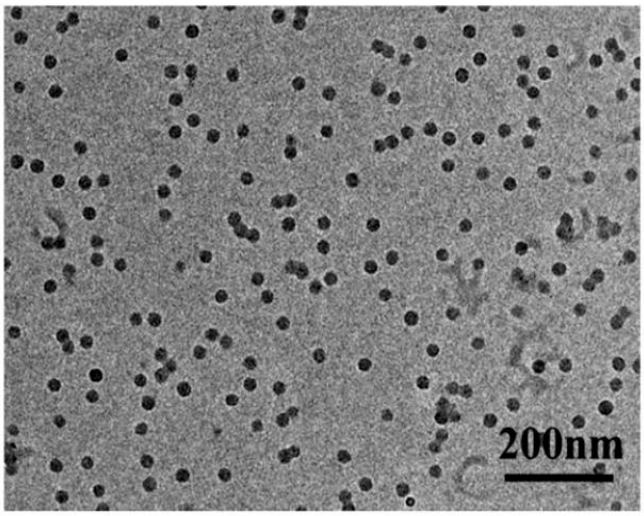

图1

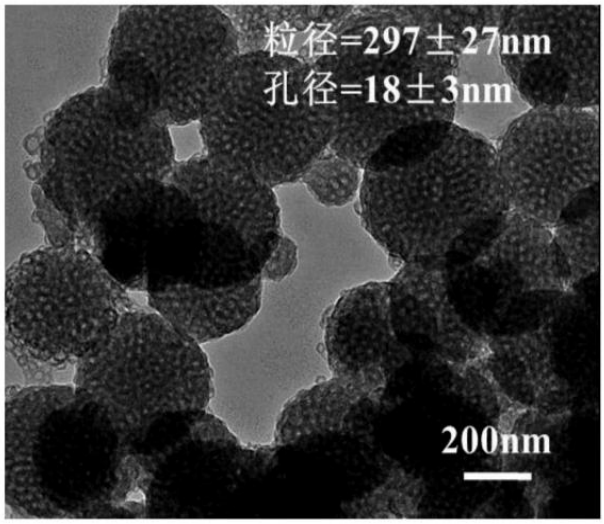

图2

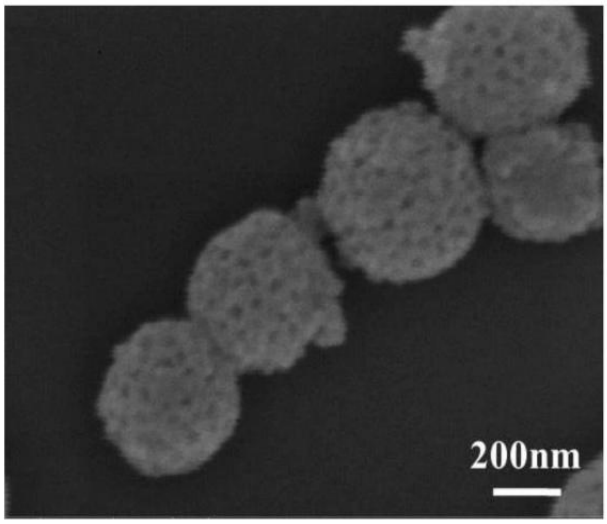
200nm

图3

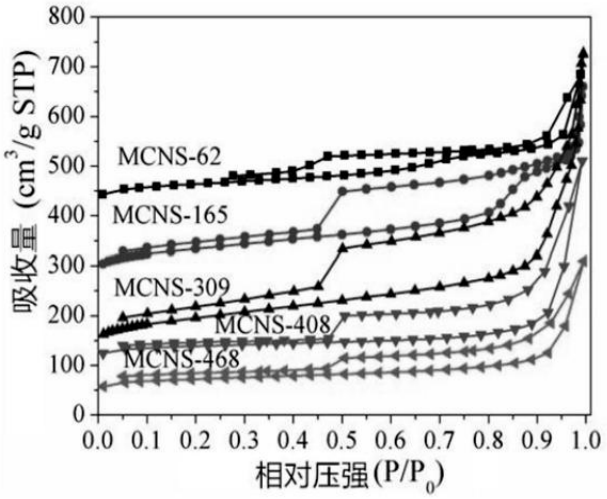
800
700
600
500
400
300
200
100
0
吸收量 (cm³/g STP)
MCNS-62
MCNS-165
MCNS-309
MCNS-408
MCNS-468
0.0 0.1 0.2 0.3 0.4 0.5 0.6 0.7 0.8 0.9 1.0
相对压强(P/P0)

图4

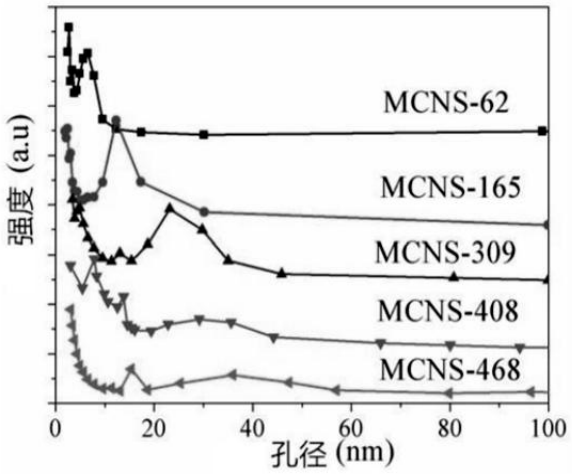
MCNS-62
MCNS-165
MCNS-309
MCNS-408
MCNS-468
强度 (a.u)
0
20
40
60
80
100
孔径 (nm)

图5

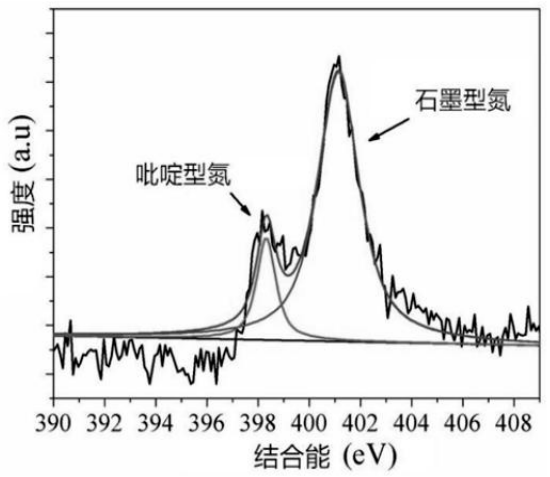
石墨型氮
吡啶型氮
强度 (a.u)
390 392 394 396 398 400 402 404 406 408
结合能 (eV)

图6

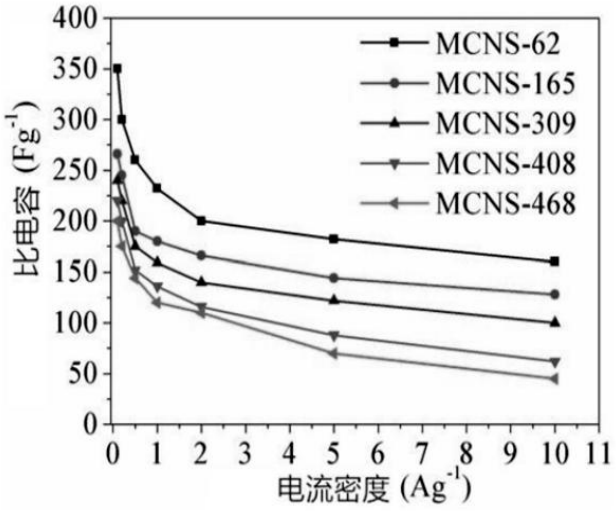
MCNS-62
MCNS-165
MCNS-309
MCNS-408
MCNS-468
比电容 (Fg-1)
电流密度 (Ag-1)
0
50
100
150
200
250
300
350
400
0 1 2 3 4 5 6 7 8 9 10 11

图7

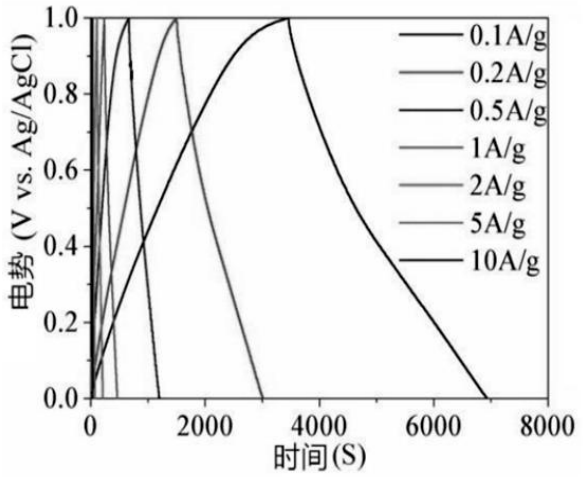
0.1A/g
0.2A/g
0.5A/g
1A/g
2A/g
5A/g
10A/g
电势 (V vs. Ag/AgCl)
时间(S)
0.0
0.2
0.4
0.6
0.8
1.0
0
2000
4000
6000
8000

图8

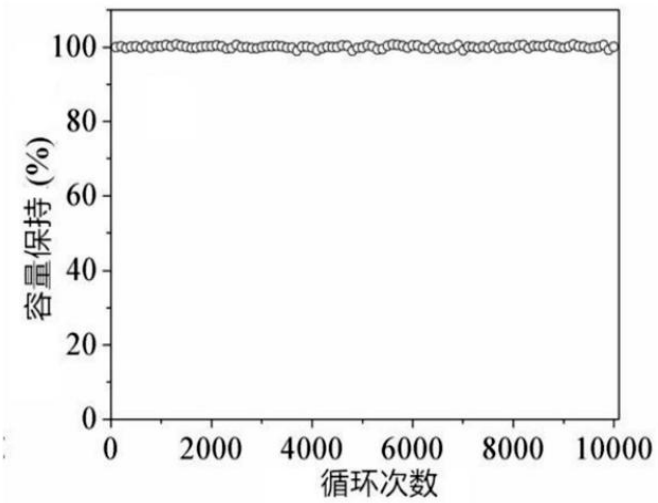

图9